HHS Public Access

Author manuscript

Nat Cancer. Author manuscript; available in PMC 2023 April 12.

Published in final edited form as:

Nat Cancer. 2021 January ; 2(1): 83–97. doi:10.1038/s43018-020-00147-8.

Targeting PAK4 to reprogram the vascular microenvironment and improve CAR-T immunotherapy for glioblastoma

Wenjuan Ma[1,8,9], **Yanling Wang**[1,9], **Rongxin Zhang**[1,8,9], **Fan Yang**[1,9], **Duo Zhang**[1], **Menggui Huang**[1], **Lin Zhang**[2], **Jay F. Dorsey**[1], **Zev A. Binder**[3,4], **Donald M. O'Rourke**[3,4], **Joseph A. Fraietta**[5,6], **Yanqing Gong**[7,10,✉], **Yi Fan**[1,3,4,10,✉]

[1]Department of Radiation Oncology, University of Pennsylvania, Philadelphia, PA, USA.

[2]Department of Obstetrics and Gynecology, University of Pennsylvania, Philadelphia, PA, USA.

[3]Department of Neurosurgery, University of Pennsylvania, Philadelphia, PA, USA.

[4]Glioblastoma Translational Center of Excellence, Abramson Cancer Center, University of Pennsylvania, Philadelphia, PA, USA.

[5]Department of Microbiology, University of Pennsylvania, Philadelphia, PA, USA.

[6]Center for Cellular Immunotherapies, Abramson Cancer Center, University of Pennsylvania, Philadelphia, PA, USA.

[7]Division of Translational Medicine and Human Genetics, Department of Medicine, University of Pennsylvania, Philadelphia, PA, USA.

[8]Present address: State Key Laboratory of Oncology in South China and Collaborative Innovation Center for Cancer Medicine, Sun Yat-sen University Cancer Center, Guangzhou, China.

[9]These authors contributed equally: Wenjuan Ma, Yanling Wang, Rongxin Zhang, Fan Yang.

[10]These authors jointly supervised this work: Yanqing Gong, Yi Fan.

Abstract

Malignant solid tumors are characterized by aberrant vascularity that fuels the formation of an immune-hostile microenvironment and induces resistance to immunotherapy. Vascular abnormalities may be driven by pro-angiogenic pathway activation and genetic reprogramming

✉ gongy@pennmedicine.upenn.edu; yi.fan@pennmedicine.upenn.edu. **Correspondence and requests for materials** should be addressed to Y.G. or Y.F.

Author contributions

W.M. performed the kinome screening analysis, RNA-seq and animal studies with transgenic mice. Y.W. and F.Y. conducted the mechanistic studies and CAR-T therapy work. R.Z. performed the cell function experiments. D.Z. conducted the three-dimensional vasculature imaging. M.H. generated the screening constructs. D.Z. and L.Z. contributed to the bioinformatics analysis. J.F.D. contributed to the experimental design. Z.A.B. and D.M.O. contributed to preparation of the cells derived from patients with GBM. J.A.F. helped to design the CAR-T therapy. Y.G. and Y.F. designed and co-supervised the experiments. Y.F. conceived of the ideas and wrote the manuscript. All of the authors commented on the manuscript.

Competing interests

Y.F. is an inventor on a patent application covering the use of PAK4 inhibitors for vessel normalization therapy. L.Z. received research funding from AstraZeneca, Bristol-Myers Squibb/Celgene and Prelude Therapeutics.

Extended data is available for this paper at https://doi.org/10.1038/s43018-020-00147-8.

Supplementary information is available for this paper at https://doi.org/10.1038/s43018-020-00147-8.

in tumor endothelial cells (ECs). Here, our kinome-wide screening of mesenchymal-like transcriptional activation in human glioblastoma (GBM)-derived ECs identifies p21-activated kinase 4 (PAK4) as a selective regulator of genetic reprogramming and aberrant vascularization. PAK4 knockout induces adhesion protein re-expression in ECs, reduces vascular abnormalities, improves T cell infiltration and inhibits GBM growth in mice. Moreover, PAK4 inhibition normalizes the tumor vascular microenvironment and sensitizes GBM to chimeric antigen receptor–T cell immunotherapy. Finally, we reveal a MEF2D/ZEB1- and SLUG-mediated mechanism by which PAK4 reprograms the EC transcriptome and downregulates claudin-14 and VCAM-1 expression, enhancing vessel permeability and reducing T cell adhesion to the endothelium. Thus, targeting PAK4-mediated EC plasticity may offer a unique opportunity to recondition the vascular microenvironment and strengthen cancer immunotherapy.

T cell-based immunotherapy for solid tumors is currently limited by efficacy challenges, largely due to tumor microenvironment-dependent therapeutic resistance. The tumor vasculature is structurally and topologically abnormal, which impedes the delivery of T cells into the tumor[1–4]. Moreover, tumor-associated endothelial cells (ECs) with functional abnormalities induce heterogeneous hypoxia and form a vascular niche that induces immune suppression[5–9], further contributing to tumor evasion of immune responses and inducing tumor resistance to immunotherapies. As such, targeting tumor ECs in order to normalize vessel delivery and rectify endothelial functions may stimulate T cell recruitment to and persistence in the tumor, serving as an emerging strategy for cancer therapy[3,4]. However, current anti-vascular therapy primarily involves targeting pro-angiogenic pathways, such as by vascular endothelial growth factor blockade, which has shown small effects on vessel normalization, exhibiting transient benefits in treating most malignant cancers[10–12]. As an alternative process to the vascular abnormality mechanism driven by angiogenic factor-mediated vessel sprouting and outgrowth, ECs undergo cell plasticity-mediated genetic reprogramming to induce aberrant vascularity in the tumor microenvironment (for example, ECs acquire mesenchymal-like transcriptional activation (endothelial transformation or partial mesenchymal transition) to promote their ability to proliferate, migrate and secrete[13,14], serving as a potential target for reconditioning the tumor microenvironment to improve cancer immunotherapy[15]).

Glioblastoma (GBM)—the grade IV glioma—is the most common and most aggressive malignant primary brain tumor. GBM is among the most lethal of human malignancies, with a current median survival of approximately 14–16 months. GBM is distinguished by prominent vascularity and extraordinary vessel abnormality[16,17]. GBM tumors exhibit high resistance to cytotoxic treatments and to anti-angiogenic therapies[10,12,17–20]. Consistent with its immunologically cold nature, GBM is also relatively refractory to T cell-based immunotherapies, including programmed cell death protein 1/programmed death-ligand 1-targeting checkpoint inhibition and adoptive cell transfer with chimeric antigen receptor (CAR)-modified T cells, largely due to an immune-hostile microenvironment with aberrant vasculature that inhibits T cell infiltration and activation[21–24]. Here, our kinome-wide functional screening of cell plasticity with human GBM-derived ECs identifies p21-activated kinase 4 (PAK4) as a driver of genetic reprogramming and aberrant vascularity. Importantly, PAK4 inhibition normalizes the tumor vascular microenvironment and improves CAR-T

immunotherapy in mouse GBM models. Thus, targeting PAK4 may provide a much-needed opportunity to improve T cell-based cancer immunotherapy.

Results

Kinome-wide genetic screening of mesenchymal-like transcriptional activation identifies PAK4 as a critical regulator of cell abnormalities in GBM ECs.

We performed a kinome-wide genetic screen to identify kinases that regulate mesenchymal-like transcriptional activation in human GBM tumor-derived ECs. GBM ECs were lentivirally transduced to express genetic probes by which the expression of firefly and renilla luciferases (fLuc and rLuc) was controlled by the promoters of α-smooth muscle actin (α-SMA, a mesenchymal gene robustly overexpressed in GBM ECs but not normal ECs[13,14]) and cytomegalovirus (CMV, as a control), respectively, followed by secondary lentiviral transduction with a multiplexed short hairpin RNA (shRNA) library that targets the human kinome (Fig. 1a). We initially identified 35 candidate kinases that potentially induce mesenchymal transcriptional activation in GBM ECs (Fig. 1b). Among them, PAK4 was the top candidate in the list (Fig. 1c). Furthermore, five individual PAK4 shRNAs consistently and robustly inhibited α-SMA transcription, which was not observed using shRNAs that target other PAK family members (Fig. 1d). Although PAK2 is a major regulator of cell functions in normal ECs[25–27], PAK2 shRNAs moderately reduced α-SMA transcription by about 40% in GBM ECs, in contrast with 70% reduction induced by PAK4 shRNAs. These results were confirmed by CRISPR–Cas9- and small interfering RNA (siRNA)-mediated knockdown of PAK4 (Fig. 1e,f and Extended Data Fig. 1a,b). PAK4 knockdown inhibited cell proliferation, migration and invasion (Fig. 1g–i) and reduced monolayer permeability (Fig. 1j) in GBM ECs. siRNA-mediated PAK4 knockdown inhibited cell proliferation and migration in GBM ECs derived from multiple human patients, but not in normal brain ECs (Extended Data Fig. 1c–f), suggesting a pathologically selective effect. Notably, PAK4 knockdown induced a cell morphology shift from the mesenchymal cell-like, spindle-shaped appearance to characteristic cobblestone cells in GBM ECs, and normalized their tube-like structure in Matrigel (Fig. 1k). Together, these results suggest that PAK4 is a selective regulator of functional abnormalities in GBM ECs.

Genetic PAK4 ablation reduces EC abnormalities, improves T cell infiltration and inhibits GBM development.

To determine the in vivo role of PAK4 in tumor vascularization, we generated an EC-specific PAK4 knockout mouse line called *Cdh5-Cre*^{ERT2};*Pak4*$^{fl/fl}$ by crossing *Pak4*$^{fl/fl}$ mice with mice expressing Cre under the EC-specific promoter *Cdh5* (Fig. 2a). EC-specific PAK4 knockout was verified by immunoblot analysis (Fig. 2b). Interestingly, PAK4 deficiency did not affect the proliferation or migration of normal ECs (Extended Data Fig. 2a,b) or other basal functions such as angiogenesis, as indicated by apparently normal body growth (Extended Data Fig. 2c), suggesting that endothelial PAK4 plays a dispensable role with regard to normal EC function and physiological angiogenesis in adults.

We then challenged these mice with an orthotopic injection of the tumor cells isolated from a replication-competent avian sarcoma-leukosis (RCAS) virus–mediated genetically

engineered GBM model (Fig. 2c). Our results showed that the EC-specific PAK4 knockout substantially improved animal survival (Fig. 2d). Notably, approximately 80% of PAK4 knockout mice survived for at least 60 d after the experiment was terminated, whereas all wild-type mice died within 40 d after tumor implantation. Similarly, PAK4 knockout robustly inhibited tumor growth (Fig. 2e). Furthermore, PAK knockout reduced intratumoral hypoxia and vascular abnormality, as indicated by a vascular morphology shift from dilated and tortuous features to normalized vessels (Fig. 2f). Consistent with the potential role of PAK4 in mesenchymal transcriptional activation in ECs, PAK4 knockout inhibited expression of the mesenchymal protein fibroblast-specific protein 1 (FSP-1) and restored expression of the adhesion protein vascular cell adhesion molecule 1 (VCAM-1) in tumor-associated ECs (Extended Data Figs. 3 and 4). Interestingly, PAK4 knockout robustly stimulated T cell infiltration into the tumors (Fig. 2g), probably contributing to the inhibition of tumor growth. To verify this, tumor-bearing wild-type or PAK4 knockout mice were intravenously infused with T cells expressing rLuc-tdTomato, followed by T cell imaging (Fig. 2h). Whole-body bioluminescence analysis showing that PAK4 knockout dramatically improved $rLuc^+$ T cell homing into the tumors (Fig. 2i,j). Together, these findings suggest that endothelial PAK4 is critical for EC functional abnormalities, T cell infiltration and tumor development.

PAK4 inhibition inhibits proliferation in GBM ECs and normalizes the tumor vasculature.

We investigated the effects of pharmacological PAK4 inhibition on EC functions and vascular morphology in GBM. Treatment with KPT9274—a selective inhibitor of PAK4—specifically inhibited the proliferation of ECs derived from GBM tumors, but not from normal brain (Fig. 3a,b). Similar results were observed following treatment with PF3758309—a pan-PAK inhibitor—suggesting a pathologically selective effect of PAK4 in tumor ECs (Fig. 3c). To determine in vivo effects of PAK4 inhibition, GBM was induced in *Cdh5-Cre*^{ERT2};*Rosa-LSL-tdTomato* mice in which tdTomato was specifically expressed in ECs, followed by administration of KPT9274 (Fig. 3d). We took advantage of light sheet fluorescence imaging technology that allowed us to visualize the vasculature at the whole-organ level. Our data showed that KPT9274 apparently altered the chaotic morphology (tortuous and discontinuous vessels with spatial heterogeneity) and resulted in a well-organized structure (continuous vessels) in the tumor-associated vasculature (Fig. 3e and Supplementary Video 1). Moreover, KPT9274 treatment led to a marked reduction in intratumoral hypoxia (Fig. 3f and Supplementary Video 2), suggesting reconditioning of the tumor microenvironment. In support of these findings, administration of PF3758309 also led to reduced EC abnormalities in mouse GBM (Fig. 3g).

PAK4 regulates mesenchymal-like transcription in GBM ECs.

We investigated the potential mechanisms by which PAK4 regulates EC plasticity and vascular abnormalities at the transcriptome level. Immunoblot and RNA sequencing (RNA-seq) analyses verified selective knockdown of PAK4 over other PAKs in ECs isolated from three human GBM tumors (Fig. 4a). Interestingly, PAK4 knockdown induced a potential lineage switch in GBM ECs (Fig. 4b), together with an altered global gene expression profile (Fig. 4c,d). Specifically, PAK4 knockdown reduced the expression of several mesenchymal genes, such as *S100A4* (FSP-1), *ACTA2* (α-SMA) and *CDH2* (N-cadherin)

in GBM ECs (Fig. 4e). PCR with reverse transcription (RT-PCR) analysis confirmed the critical role of PAK4 for FSP-1 expression in GBM ECs (Fig. 4f). Considering the key role of transcription repressors, including Snail, Slug, transcription factor 3 (Tcf3), Twist1/2 and zinc finger E-box-binding homeobox 1/2 (Zeb1/2), for the epithelial–mesenchymal transition (EMT) in epithelium[28–30], we analyzed their expression in GBM ECs. Our data showed that PAK4 knockdown attenuated the expression of SLUG, TCF3, TWIST1/2 and ZEB1 in GBM ECs (Fig. 4g). In accordance with these results, immunoblot analysis showed that PAK4 knockdown inhibited the expression of FSP-1, α-SMA, SLUG and ZEB1 in GBM ECs (Fig. 4h), suggesting that PAK4 is critical for mesenchymal-like transcriptional activation in tumor ECs, which probably induces aberrant vascularity in GBM.

PAK4 suppresses claudin-14 transcription via ZEB1 expression, enhancing vessel permeability.

Next, we explored the molecular mechanism(s) underlying PAK4-mediated mesenchymal-like transcriptional activation, focusing on tight and adherens junctions, which play critical roles in EMT initiation. RNA-seq analysis of GBM ECs revealed that PAK4 knockdown enhanced the expression of multiple adhesion-associated genes, with claudin-1/14, occludin and Jam-2 at the top of the list (Fig. 5a). Immunoblot analysis verified that PAK4 knockdown increased the expression of claudin-1/14, but not the expression of claudin-4/5, CD31 (*PECAM1*), occludin or Jam-2 in GBM ECs, rather than normal brain ECs (Fig. 5b and Extended Data Fig. 5), suggesting a pathologically specific role of PAK4 in cell dissociation in tumor ECs. Considering that PAK4 induced ZEB1 and Slug expression (Fig. 4h), we investigated the role of these two transcriptional repressors in PAK4-regulated claudin-1/14 expression. Interestingly, siRNA-mediated knockdown of ZEB1, but not of SLUG, partially restored claudin-14 expression in GBM ECs (Fig. 5c,d), suggesting that ZEB1 inhibits claudin-14 expression. Similarly, chromatin immunoprecipitation (ChIP) analysis showed that ZEB1 was bound to the claudin-14 promoter in GBM ECs but not in normal ECs (Fig. 5e). Furthermore, knockdown of either ZEB1 or PAK4 reduced monolayer permeability in GBM ECs (Fig. 5f). Together, these findings suggest that PAK4 induces ZEB1 expression, leading to downregulation of claudin-14 expression and disruption of cell junctions while also contributing to EC mesenchymal phenotypes, including high permeability.

PAK4 downregulates intercellular adhesion molecule 1 (ICAM-1) and VCAM-1 expression via SLUG, reducing T cell adhesion to GBM ECs.

Downregulated expression of adhesion proteins, including ICAM-1, VCAM-1 and E-selectin, in tumor ECs reduces T cell adhesion to the vasculature, inhibiting inflammatory cell infiltration into the tumors[31–33]. We tested the possible role of PAK4 in regulating the expression of these adhesion proteins in ECs. RNA-seq analysis of GBM ECs showed that PAK4 knockdown induced twofold increases in VCAM-1 and ICAM-1 (Fig. 5a), in accordance with our findings showing that PAK4 knockout enhances VCAM-1 expression in tumor ECs (Extended Data Fig. 4). Immunoblot data verified the downregulated expression of ICAM-1 and VCAM-1 in GBM ECs and, more importantly, showed that knockdown of PAK4 partially rescued the expression of ICAM-1 and VCAM-1 in GBM ECs but did not affect their expression in normal ECs (Fig. 5b). Moreover, knockdown of SLUG or, to a

lesser extent, ZEB1 in GBM ECs partially rescued the expression of ICAM-1 and VCAM-1 (Fig. 5c,d). Consistent with their important role in the regulation of T cell interactions with ECs, knockdown of PAK4 or SLUG enhanced T cell binding to the GBM ECs (Fig. 5g). These data collectively suggest an additional role for PAK4/SLUG in the regulation of T cell adhesion to endothelium via ICAM-1 and VCAM-1.

PAK4 induces myocyte-specific enhancer factor 2D (MEF2D)-dependent ZEB1 expression in GBM ECs.

To gain molecular insights into the PAK4-mediated regulation of ZEB1 expression, we performed a computational bioinformatics analysis of the top 500 downregulated gene promoter sequences in PAK4 knockdown GBM ECs. Our results uncovered consensus DNA motifs that are known to be recognized by multiple transcription factors (Fig. 6a). Furthermore, our multiplex analysis of transcriptional activation identified several transcription factors with increased activity in GBM ECs relative to normal ECs (Fig. 6b). Considering the overlapping transcription factors in these two lists and previous literature, we focused on MEF2, lymphoid enhancer-binding factor 1 (LEF1) and peroxisome proliferator-activated receptor-γ (PPARγ). In accordance with a previous report showing that MEF2D regulates ZEB1 expression in tumor cells[34], treatment of GBM ECs with siRNA targeting MEF2D, but not with siRNAs targeting LEF1 or PPARγ, markedly abrogated ZEB1 expression instead of SLUG expression (Fig. 6c). Consistent with the role of MEF2 in regulating ZEB1 expression, our ChIP analysis verified MEF2 binding to the ZEB1 promoter in GBM ECs (Fig. 6d). Furthermore, PAK4 siRNA reduced the interaction between MEF2D and the ZEB1 promoter (Fig. 6d). Similarly, PAK4 siRNA reduced MEF2 transcriptional activity in GBM ECs (Fig. 6e). These findings suggest that PAK4 promotes MEF2D binding to the ZEB1 promoter and induces Zeb1 expression in GBM ECs.

In addition, expression of wild-type PAK4, but not the kinase-dead PAK4 with a p.Lys350Met alteration ($PAK4^{K350M}$), robustly stimulated expression of the mesenchymal proteins SLUG, ZEB1 and FSP-1 and suppressed expression of the adhesion proteins ICAM-1 and claudin-14 in PAK4 knockdown GBM ECs (Extended Data Fig. 6a). Moreover, re-expression of wild-type PAK4, but not $PAK4^{K350M}$, partially rescued cell proliferation and migration in PAK4 knockdown GBM ECs (Extended Data Fig. 6b,c), suggesting a critical role of PAK4 kinase activity in mesenchymal-like transcriptional reprogramming and cell functions in tumor ECs. Furthermore, our data showed that PAK4 knockdown abrogated MEF2D phosphorylation at Ser^{180}, rather than Ser^{444}, in GBM ECs, which could be rescued by re-expression of wild-type PAK4, but not $PAK4^{K350M}$ (Extended Data Fig. 7a). Consistent with these findings, purified recombinant PAK4 protein induced MEF2D phosphorylation at Ser^{180} in vitro (Extended Data Fig. 7b). These data suggest that PAK4 kinase activity is critical for mesenchymal-like phenotypes in GBM ECs, and that this is mediated, at least partially, through PAK4 phosphorylation of MEF2D at Ser^{180}.

PAK4 inhibition improves CAR-T immunotherapy in two mouse GBM models.

Based on our observation that PAK4 deficiency in ECs led to tumor microenvironment reconditioning and enhanced T cell infiltration into the tumors, and that PAK4 inhibition normalized the tumor vasculature, we next investigated the effects of PAK4 inhibition

on CAR-T immunotherapy. We developed a murine CAR-T system in which mouse T cells were retrovirally transduced to express a murine CAR construct containing a 139 scFv that targets EGFRvIII—a GBM-associated epidermal growth factor receptor (EGFR) mutant[35] (Extended Data Fig. 8a). The transduced T cells exhibited selective cytotoxicity against tumor cells that express mouse Egfrviii but not wild-type Egfr (Extended Data Fig. 8b,c). We then administrated CAR-T immunotherapy in mice bearing Egfrviii-expressing syngeneic GL261 GBM tumors following KPT9274 treatment (Fig. 7a). Our data showed that KPT9274 treatment did not significantly inhibit tumor growth ($P > 0.1$ relative to the saline-treated group; Fig. 7b), nor did it improve mouse survival ($P > 0.05$; Fig. 7c). Furthermore, CAR-T immunotherapy alone also failed to affect tumor growth and mouse survival (Fig. 7c), consistent with limited basal cell infiltration after T cell infusion (Fig. 2g,j). In contrast, KPT9274 treatment sensitized tumors to CAR-T immunotherapy, as indicated by an approximately 80% reduction in tumor volume at 5 d after CAR-T cell infusion (Fig. 7b). As such, the combination therapy significantly enhanced mouse survival ($P < 0.01$; Fig. 7c). Notably, nearly 40% of the mice in the combination therapy group still survived even when all of the mice in the other groups had died by 33 d after tumor induction (Fig. 7c). To further test the immunotherapy in a setting that recapitulates human GBM, GBM was genetically induced in donor mice, and tumor spheres were retrovirally transduced to express mouse Egfrviii before implantation into recipient mice, leading to Egfrviii expression in approximately one-third of the tumor cells (Fig. 7d and Extended Data Fig. 9), which is comparable to human patients with GBM. Similar to the responses in the syngeneic GL261 model, neither Egfrviii CAR-T therapy nor KPT9274 treatment alone inhibited tumor growth or improved mouse survival in the genetic Egfrviii GBM model (Fig. 7e,f). However, combination therapy with Egfrviii CAR-T therapy and KPT9274 delayed tumor growth and increased mouse survival. Together, these results indicate that PAK4 inhibition sensitizes GBM tumors to CAR-T immunotherapy.

Taken together, the results of our experiments identify PAK4 as a critical regulator of EC abnormalities in GBM (Fig. 7g). We uncovered a PAK4-mediated mechanism that downregulates adhesion protein expression and induces mesenchymal-like transcriptional activation in GBM ECs, driving abnormal cell phenotypes and aberrant tumor vascularization, which leads to the formation of an immune-hostile microenvironment that inhibits T cell adhesion to endothelium and infiltration into tumors. We show that PAK4 inhibition normalizes the tumor vascular microenvironment and improves CAR-T immunotherapy in mouse GBM models.

Discussion

Immunotherapy by adoptive T cell transfer with CAR-T cells holds great promise for treating solid tumors, including GBM[36–38]. However, CAR-T immunotherapy of solid tumors has encountered major difficulties and failures in the clinic, largely due to limited T cell infiltration and activation in the tumor microenvironment, particularly for immunologically cold tumors such as GBM[22]. Likewise, normalization of the aberrant vascular microenvironment represents a promising strategy for improving immunotherapy by promoting the delivery of T cells through vessels that infiltrate the tumors. Moreover, inhibition of mesenchymal-like plasticity in tumor ECs may abrogate their

immunosuppressive mesenchymal phenotypes[5,39], contributing to the formation of a T cell-favorable vascular microenvironment. Furthermore, down-expression of adhesion proteins in tumor ECs impedes leukocyte adhesion to, and diapedesis through, the tumor vessel wall, as one of the mechanisms tumors have developed to escape the immune response[31–33]; therefore, functionally programming tumor ECs to restore adhesion protein expression may improve T cell recruitment to the tumors and stimulate anti-tumor immunity. In the present study, we utilized endothelial plasticity-based genetic screening to identify PAK4 as a regulator of EC functional abnormalities in cancer. Our study reveals that PAK4-targeted therapy restores adhesion protein expression in GBM ECs and normalizes the vascular microenvironment, thereby enhancing T cell homing to the tumor and sensitizing GBM to CAR-T immunotherapy. In addition, our findings provide support for the idea that structural vessel normalization by PAK4 inhibition can also improve drug delivery and reduce intratumoral hypoxia, leading to improved tumor responses to molecular targeted therapy and radio-/chemotherapy.

Cell plasticity in ECs has been well characterized in embryogenesis and pathological settings, including cardiac, renal and liver fibrosis, pulmonary hypertension, vascular inflammation and cerebral cavernous malformation[40–51]. Our recent work shows that GBM-associated ECs exhibit robust cell plasticity to acquire mesenchymal phenotypes including enhanced proliferation and motility via stimulus-dependent hepatocyte growth factor/Ets-1- and platelet-derived growth factor (PDGF)/Snail-mediated mechanisms, leading to aberrant vascularization[13–15]. Here, we uncover PAK4 as a regulatory node that intrinsically reprograms the transcriptome in tumor ECs and suppresses adhesion protein expression via ZEB1 and SLUG, contributing to the formation of an aberrant, T cell-inhibitory microenvironment. It is well known that ZEB1 and SLUG act as transcription factors that repress E-cadherin expression and induce EMT[29,52–54]. Our data suggest that ZEB1 downregulates expression of the tight junction protein claudin-14 through a PAK4/MEF2D-mediated mechanism, probably contributing to the initiation of EC plasticity. In accordance with these findings, a previous study showed that MEF2D induces ZEB1 expression to activate EMT[34].

In contrast with the classical role for PAK4 in cell migration and polarity[55], we found that PAK4 drives mesenchymal-like transcription activation in tumor ECs, which induces functional EC abnormalities. Recent work also showed that PAK4 regulates EMT through Nox1 in colon cancer and glioma cells[56,57]. Interestingly, previous studies suggested that PAKs function as downstream nodes for various oncogenic signaling pathways in tumor cells[58]. As such, recent studies showed that PAK4 inhibition may disrupt Wnt/β-catenin signaling in tumor cells and activate tumor immunity, resulting in stimulated T cell proliferation in the tumor, as well as improved tumor response to immune checkpoint inhibition[59,60], which provides additional benefits for PAK4-targeted cancer therapy. Nevertheless, our findings using pharmacological inhibition and conditional genetic ablation reveal selective microenvironment-mediated effects of PAK4 inhibition on immunotherapy, which is also supported by time-dependent therapeutic effects induced by CAR-T immunotherapy after PAK4 inhibition. We suggest that the therapeutic efficacy associated with enhanced T cell delivery and homing by PAK4 inhibition can be further improved when combined with other immunotherapy approaches capable of increasing T

cell persistence by inhibiting T cell exhaustion and/or by stimulating T cell activation in the tumor microenvironment. In addition, we show that PAK4 inhibition plus CAR-T therapy prolonged survival in GBM-bearing mice in a condition without lymphodepletion chemotherapy, representing an additional benefit for this combination therapy.

In summary, our work uncovers a previously unknown system that reprograms tumor ECs to induce abnormal EC functions and aberrant vascularization, and suggests that targeting PAK4-mediated EC plasticity may provide a unique opportunity to recondition the tumor microenvironment and improve immunotherapy for treating solid tumors.

Methods

EC isolation from patient tumors.

Human patient samples were collected at the Department of Neurosurgery of the University of Pennsylvania. The collection of human tissues, in compliance with the tissue banking protocol, was approved by the University of Pennsylvania Institutional Review Board, and written informed consent was obtained from each participant[13,14]. ECs were isolated and verified as previously described[13,14]. In brief, tumor-derived single-cell suspensions were prepared by the tissue bank. Cell suspensions were subjected to magnetic-activated cell sorting using anti-CD31 antibody-conjugated magnetic beads (1:100; Miltenyi Biotech; 130-091-935). Sorted ECs were verified by Dil-Ac-LDL (Alfa Aesar; J65597) absorption and von Willebrand factor staining.

Mice.

Cdh5-Cre^{ERT2};*Rosa-LSL-tdTomato* mice were generated by crossing *Rosa-LSL-tdTomato* mice (The Jackson Laboratory) with *Cdh5-Cre*^{ERT2} mice (kindly provided by R. Adams at Max Planck)[61]. *Cdh5-Cre*^{ERT2};*Pak4*$^{fl/fl}$ mice were generated by crossing *Pak4*$^{fl/fl}$ mice (generated by A. Minden at Rutgers and purchased from The Jackson Laboratory) with *Cdh5-Cre*^{ERT2} mice. All animals were housed at room temperature with a 12-h light/12-h dark cycle at an Association for Assessment and Accreditation of Laboratory Animal Care-accredited animal facility of the University of Pennsylvania. All experiments with mice were performed in accordance with an animal protocol approved by the Institutional Animal Care and Use Committee at the University of Pennsylvania.

Isolation and culture of mouse ECs.

Mouse aorta ECs were isolated and cultured as previously described[13,14]. In brief, thoracic aortas were isolated from 3-week-old *Cdh5-Cre*^{ERT2};*Pak4*$^{fl/fl}$ and *Pak4*$^{fl/fl}$ mice. Aortic rings were embedded in Matrigel-coated dishes and cultured for 5 d. The rings were removed and the remaining cells were incubated with 2 U ml^{-1} Dispase I (Gibco; 17105-041) for 20 min at 37°C. After centrifugation at 500*g* for 10 min, the cell pellets were washed with phosphate-buffered saline (PBS) and the cells were cultured in Dulbecco's modified Eagle's medium/F-12 medium supplemented with 25 μg ml^{-1} EC growth supplement (Sigma–Aldrich) and 5% fetal bovine serum (FBS) at 37°C under a humidified air atmosphere with 5% CO_2.

Tissue protein extraction.

The hearts were excised from *Cdh5-Cre*^{ERT2};*Pak4*$^{fl/fl}$ and *Pak4*$^{fl/fl}$ mice. Tissues were collected and homogenized in PBS with proteinase inhibitor cocktail (Roche; 11697498001), followed by tissue lysis with NP-40 buffer.

GBM mouse models and treatment.

Genetically engineered GBMs were induced in mice as described previously[13,62–64]. In brief, chicken DF-1 fibroblasts (American Type Culture Collection) were transfected with RCAS-PDGF-B and RCAS-Cre plasmids to produce retrovirus, followed by orthotopic injection into *Ntv-a*;*Ink4a-Arf*$^{-/-}$;*Pten*$^{fl/fl}$;*LSL-luc* mice to induce GBM. Tumors were isolated and subjected to mechanical dissociation with a gentleMACS Dissociator (Miltenyi Biotec) and enzymatic digestion using collagenase II and dispase II to obtain single-cell suspensions. For retroviral transduction, medium supernatant was collected from DF-1 cells that were transfected to express RCAS-mouse Egfrviii. After centrifugation, the virus pellet was suspended in mouse stem cell medium and incubated with tumor-derived sphere cells. Approximately 8-week-old mice (half male and half female) were orthotopically and stereotactically injected with 10^5 GBM tumor cells. For the syngeneic GBM model, mouse GL261 glioma cells were lentivirally transduced to co-express mouse Egfrviii and green fluorescent protein, and green fluorescent protein-positive cells were harvested by cell sorting. A total of 2×10^5 cells in a total volume of 2 μl were orthotopically injected into wild-type C57/B6 mice. Tumor growth was monitored by bioluminescence using an IVIS 200 Spectrum Imaging System (PerkinElmer) after retro-orbital injection of luciferin (150 mg kg^{-1}; GoldBio). For tumor induction in *Cdh5-Cre*^{ERT2};*Pak4*$^{fl/fl}$ and *Cdh5-Cre*^{ERT2};*Rosa-LSL-tdTomato* mice, tumor-derived single-cell suspensions were cultured with NeuroCult mouse stem cell medium (Stemcell Technologies). Attached cells were discarded to remove tumor stromal cells, and non-adherent sphere-forming tumor cells were injected into mouse brains. For T cell imaging, mice were injected with mouse T cells expressing tdTomato-rLuc (2×10^6 cells per mouse) through the tail vein after GBM induction. Mice were imaged after retro-orbital injection of coelenterazine (4 mg kg^{-1}; Promega), followed by secondary imaging after retro-orbital injection of D-luciferin (150 mg kg^{-1}; GoldBio). Mice were administrated a peritoneal injection of saline, 20 mg kg^{-1} KPT9274 (Selleckchem), 20 mg kg^{-1} PF3758309 (Selleckchem) or CAR-T cells (5×10^6 cells per mouse) through the tail vein after GBM induction. Post-injection survival was monitored for up to 60 d. Mice were euthanized when exhibiting severe GBM symptoms including domehead, hemiparesis or more than 20% of body weight loss. Mice were randomized to receive treatment and the investigators were not blinded.

Flow cytometry.

Single-cell suspensions derived from RCAS-Egfrviii tumors were stained with control immunoglobulin G (IgG) or anti-Egfrviii antibody (1:100; Millipore; MABS1915), followed by incubation with fluorescence dye-conjugated secondary antibody (1:500; BioLegend; 406001). All of the cells were gated and analyzed using Accuri C6 (BD Biosciences) and FlowJo version 9 software.

Cell culture and treatment.

Human brain microvascular ECs (ScienCell and PromoCell, isolated from adult or fetal human brains) and GBM-derived ECs were maintained as previously described[13,14]. In brief, cells were cultured in Endothelial Cell Medium (ScienCell, supplemented with vascular endothelial growth factor A) at 37°C with 5% CO_2. All cells were used between passages two and five. Cells were treated with KPT9274 or PF3758309 (Selleckchem).

siRNA and CRISPR/single guide RNA (sgRNA) treatment.

ECs were transfected with non-targeting control siRNA (Qiagen (1027280) or Thermo Fisher Scientific (AM4611)) or with siRNAs targeting Snail (Thermo Fisher Scientific; s13185), Slug (Thermo Fisher Scientific; s13127), ZEB1 (Thermo Fisher Scientific; s229971 or 4392420), MEF2D (Dharmacon; L-009884-00-0005), LEF1 (Dharmacon; L-015396-00-0005), PPAR-γ (Dharmacon; L-003436-00-0005) or PAK4 (Thermo Fisher Scientific; s20134 or 4390824) using RNAiMAX Lipofectamine (Invitrogen; 13778075) in serum-free Opti-MEM medium (Gibco; 31985-070) for 12 h, followed by incubation with serum-supplemented medium for 24 h. The guide RNA sequence (5′-GTGTTTGGGAAGAGGAAGAAG-3′) targeting PAK4 was subcloned into lentiCRISPRv2 puro vector (Addgene; 52961). ECs were transduced with the lentivirus expressing PAK4 sgRNA, followed by cell selection by incubation with medium containing 2 μg ml^{-1} puromycin.

Plasmids and transfection.

Full-length wild-type PAK4 DNA was amplified by PCR using a human complementary DNA library and primers including 5′ AATTGGATCCATGTTTGGGAAGAGGAAGAAGC-3′ and 5′-AATTGCGGCCGCTTACTTGTCATCGTCGTCCTTGTAGTCTCTGGTGCGGTTCTGGCGCA-3′, and subcloned into pcDNA3 vector at the BamHI/NotI sites. $PAK4^{K350M}$ DNA was generated by site-directed mutagenesis (Q5 Site-Directed Mutagenesis Kit; New England Biolabs) using wild-type PAK4 as a template and primers including 5′-GGTGGCCGTCATGATGATGGACCTGCG-3′ and 5′- AGCTTGCCCGAGCTGCGC-3′. Plasmid construction was verified by restriction digestion and DNA sequencing. Cells were transfected with plasmids using Lipofectamine (Invitrogen; L3000001) in serum-free Opti-MEM medium (Gibco; 31985-070).

Cell proliferation assay.

Cell proliferation was determined as previously described[13,14]. In brief, ECs were trypsinized and seeded on 96-well plates at a density of 3,000 cells per well, and allowed to attach for 4 h. Cell proliferation was determined using the CellTiter assay (Promega; G7571) according to the manufacturer's instructions. Bioluminescence was detected using a luminescent plate reader (Synergy H4 Hybrid; BioTek).

Cell migration and invasion assay.

Cell migration was determined as previously described[13,14]. In brief, ECs were seeded at 2×10^4 cells per well on 8-μm pore insert membranes (Falcon; 353097) pre-coated with

(for the invasion assay) or without (for the migration assay) Matrigel in a 24-well plate. Cell migration was induced by the addition of 5% FBS to the bottom chamber. After a 6-h induction, ECs on the top of the membrane were swiped off with a cotton swab. Cells were fixed in methanol for 5 min and stained with Toluidine Blue O (Sigma–Aldrich; 198161) for 5 min. Images were taken in 3–4 fields per well and stained cells were counted.

EC monolayer permeability assay.

EC monolayer peameability was determined as previously described[13,14]. In brief, ECs were seeded on Transwell inserts with 0.4-μm pore membranes (Costar; 3412) in 24-well plates, and cultured for 2 d to reach confluence in phenol red-free medium. Fluorescein isothiocyanate (FITC)-conjugated dextran (molecular weight = 70,000 Da; 10 μg ml^{-1}; Santa Cruz; sc-263323) was added to the top chamber. The medium from the lower chamber was collected at different time points, and the fluorescence was measured with an excitation wavelength of 485 nm and an emission of 530 nm.

T cell adhesion assay.

Primary human $CD8^+$ T cells, obtained from the Human Immunology Core at the University of Pennsylvania, were isolated from healthy volunteer donors. All specimens were collected under a University Institutional Review Board-approved protocol, and written informed consent was obtained from each donor. T cells were labeled using a PKH67 Green Fluorescent Cell Linker Mini Kit (Sigma–Aldrich; MINI67) according to the manufacturer's instructions. T cells were added to monolayers of GBM ECs at 37°C for 24 h, followed by gentle washing with PBS to remove unattached T cells. Cells were imaged with an Axio Imager A1 fluorescence microscope (Zeiss) equipped with an Axiocam 506 charge-coupled device (CCD) camera (Zeiss). The fluorescence intensity was quantified using ImageJ software.

RNA-seq.

A total of 2×10^6 treated human tumor ECs (from the patients with GBM with IDs 5377, 5391 and 5465) were lysed in 1 ml TRIzol (Thermo Fisher Scientific), followed by RNA extraction according to the manufacturer's instructions, as previously described[14]. The isolated RNA was purified with an RNeasy Plus Mini Kit (Qiagen). After a quality control step using RNA Nano assay chips with a 2100 Bioanalyzer (Agilent), a library was constructed using a Ribo-Zero protocol with TapeStation (Agilent), and subjected to deep sequencing (125 paired-end (PE); approximately 40 MB reads for each sample; Illumina HiSeq 2500 sequencer) at the Children's Hospital of Philadelphia/Beijing Genomics Institute core facility. The sequences were aligned to the UCSC hg38 reference genome using RNA-Star (version 2.4.2a; https://github.com/alexdobin/STAR). The gene expression was normalized and calculated as fragments per kilobase of transcript per million mapped reads values by Cufflinks (version 2.2.1; http://cole-trapnell-lab.github.io/cufflinks/releases/v2.2.1/) with Gencode version 22 gene annotations (https://www.gencodegenes.org/human/release_22.html).

Real-time RT-PCR analysis.

Real-time RT-PCR was performed as previously described[13,14]. In brief, RNA was extracted with TRIzol (Invitrogen), isolated with chloroform (Sigma–Aldrich) and 2-propanol (Thermo Fisher Scientific) and subjected to reverse transcription with SuperScript III First-Strand Synthesis SuperMix (Life Technologies)[14]. Real-time PCR was performed in a 20-μl reaction volume using Fast SYBR Green Master Mix (Applied Biosystems) and the following primer sets: FSP-1 (forward: 5'-TTGGGGAAAAGGACAGATGAAG; reverse: 5'-AAGGAGCCAGGGTGGAAAAA-3′); GAPDH (forward: 5′-GTCTCCTCTGACTTCAACAGCG-3′; reverse: 5′-ACCACCCTGTTGCTGTAGCCAA-3′); and PAK4 (forward: 5′-ATCTGGTCGCTGGGGATAATG-3′; reverse: 5′-CAGGTTGTCCCGAATCATCTTC-3′).

In vitro kinase assay.

Recombinant human PAK4 (Abcam; ab96405) and MEF2D (Novus; H00004209-P01) proteins were incubated with 200 μM ATP (Cell Signaling Technology; 9804) in 40 μl 10× kinase buffer (Cell Signaling Technology; 9802) for 2 h at 30°C. The reaction was terminated by the addition of Laemmli SDS sample buffer.

Immunoblot analysis.

Cells were lysed with an NP-40 lysis buffer containing protease inhibitor cocktail (Roche; 11697498001). Cell lysate was resolved by 4–15% precast SDS-PAGE gel (Bio-Rad). After transfer, polyvinylidene difluoride membranes were blotted with the following antibodies: anti-FSP-1 (1:1,000; Millipore; 07–2274), anti-α-SMA (1:1,000; Abcam; ab5694), anti-Snail (1:1,000; Cell Signaling Technology; 3879), anti-Slug (1:1,000; Cell Signaling Technology; 9585), anti-PAK4 (1:1,000; Cell Signaling Technology; 3242), anti-PAK1 (1:1,000; Cell Signaling Technology; 2602), anti-ZEB1 (1:1,000; Cell Signaling Technology (3396) and Thermo Fisher Scientific (PA5–28221)), anti-Claudin-1 (1:1,000; Cell Signaling Technology; 13255), anti-Claudin-4 (1:1,000; Invitrogen; 32–9400), anti-Claudin-5 (1:1,000; Thermo Fisher Scientific; 35–2500), anti-Claudin-14 (1:1,000; Invitrogen; PA5–21602), anti-Occludin (1:1,000; Invitrogen; 71–1500), anti-Jam-2 (1:1,000; Invitrogen; PA5–67831), anti-ICAM-1 (1:500; Cell Signaling Technology; 67836), anti-VCAM-1 (1:500; Cell Signaling Technology; 12367), anti-PPAR-γ (1:1,000; Santa Cruz; sc-7196), anti-MEF2D (1:1,000; BD Biosciences; 610774), anti-phospho-MEF2D-Ser^{444} (1:1,000; Millipore; SAB4503938), anti-phospho-MEF2D-Ser^{180} (1:1,000; Abnova; PAB15921), anti-CD31 (1:1,000; Cell Signaling Technology; 3528), anti-LEF1 (1:1,000; Cell Signaling Technology; 2230) and anti-GAPDH (1:5,000; Cell Signaling Technology; 5174). The corresponding proteins were detected with HRP-conjugated secondary antibodies specific for either rabbit or mouse IgG (Bio-Rad), followed by enhanced chemiluminescence (ECL) development (GE Healthcare; RPN2232).

Immunofluorescence.

Immunofluorescence was performed as previously described[13,14]. In brief, mouse tumor sections were de-paraffinized and rehydrated, then subjected to antigen retrieval in Target Retrieve Solution (DAKO; S1699) at 95°C for 20 min. Sections were blocked with 5%

horse serum for 1 h at room temperature, incubated with anti-CD31 (1:100; Dianova; DIA-310; for mouse tissues), anti-FSP-1 (1:100; Millipore; 07–2274), anti-tdTomato (1:100; Rockland; 600-401-379) or anti-VCAM-1 (1:100; Cell Signaling Technology; 12367) antibody overnight at 4°C. For cell culture staining, the cells were fixed with 4% paraformaldehyde for 15 min, followed by permeabilization with 1% Triton X-100 for 5 min. Cells were blocked with 5% horse serum for 1 h, then incubated with Alexa Fluor 488-conjugated phalloidin (1:100; Invitrogen; A12379) for 20 min. Images were acquired using an Axio Imager microscope (Zeiss) equipped with an AxioCam 506 monochrome CCD camera (Zeiss).

Light sheet fluorescence imaging.

Mouse tissues were fixed in 4% paraformaldehyde overnight, then cleared according to a CLARITY protocol using the X-CLARITY Tissue Clearing System (Logos Biosystems) for 24 h, as described previously[65]. Cleared tissues were imaged using the Lightsheet Z.1 LSFM system (Zeiss). Obtained raw stack images were stitched and processed using Arivis 4D (Arivis AG) and Imaris 9.1 (Oxford Instruments) software.

Tumor hypoxia analysis.

Tumor hypoxia was determined using the Hypoxyprobe-1 Plus Kit (Hypoxyprobe) as previously descrived[13,14]. Mice were injected intravenously with pimonidazole HCl (60 mg kg^{-1}). Tumors were excised, and frozen sections were fixed with chilled acetone and stained with anti-pimonidazole adduct FITC-conjugated antibody according to the manufacturer's instructions. Sections were imaged using an Axio Imager microscope (Zeiss) equipped with an AxioCam 506 monochrome CCD camera (Zeiss). Whole tumors were analyzed by light sheet fluorescence imaging using the Lightsheet Z.1 LSFM system (Zeiss).

ChIP assay.

ChIP assays were performed using EZ-Magna ChIP Kits (Millipore; 17–408 and 17–409) as previously described[13,14]. In brief, ECs were fixed with 1% formaldehyde. Cells were collected by scratching, lysed and suspended in nuclear buffer. Five cycles of continuous sonication for 10 × 2 s were applied to break the chromatin into fragments between 100 and 500 base pairs. The samples were incubated with anti-Zeb1 antibody (1:100; Thermo Fisher Scientific; PA5–28221) or anti-MEF2D antibody (1:100; BD Biosciences; 610774) and magnetic beads overnight at 4°C. Normal IgG was used as a negative control. Immunoprecipitants were separated using a magnetic rack and washed. DNA fragments were released by incubation with proteinase K at 62°C for 2 h with continuous shaking, and were isolated by filtration. Real-time PCR was performed in a 20-μl reaction volume using Fast SYBR Green Master Mix (Applied Biosystems; 4385612) and the following primer sets of ZEB1 (forward #1: 5′-GGTATCAAGGAAAGCGAGGAC; reverse #1: 5′-TTTGTCACTTCTATGGCAGGAT; forward #2: 5′-AAATCCTGCCATAGAAGTGAC; reverse #2: 5′-TTTAGGTTTCCTTCCTGCTT; forward #3: 5′-TCATGGCCTGTGGATACCTTAGC; reverse #3: 5′-TTTGGGGACGGCGAGGA; forward #4: 5′-TCCAACTTTACCTTTCCAACTCCG; reverse #4: 5′-GCAACCGTGGGCACTGCTGAAT; forward #5: 5′-CGCCCGGTCCCTAGCAACAAGGTT; and reverse

#5: 5′-CCCCCTTCCCCCCCACCCCTC) and claudin-14 (forward #1: 5′-GCTAGGTAATCAATTCGGGTCTAA; reverse #1: 5′-CTGCAGCTAAGAATCCTTTACACA; forward #2: 5′-TCTCATTGGCCAAAGTAAGTCATA; reverse #2: 5′-TACCTAGCACAGCACTCTTCACTC; forward #3: 5′-GTGCTCATCCAAGACTACACAAGT; reverse #3: 5′-CCTGGCAAAGTCTATCTTCTGATT; forward #4: 5′-GAATAATGTGGGCTCCTCCA; reverse #4: 5′-GGAACTTGAAGAGGAGGACTGA; forward #5: 5′-GGCTGGTCTTGAACTCCTGA; reverse #5: 5′-CCCCAGTTGGACAGAAAAGA; forward #6: 5′-CGGGCTTTCTTCTGAATTTG; and reverse #6: 5′-CCCTCTCAGTACGTGCCATT).

Multiplex transcriptional activity assay.

Transcriptional activity was analyzed using a 96-well TF Protein Interaction Plate Array I kit (Signosis; FA-3001). Briefly, 10 μg nuclei extracts from ECs were isolated with a nuclear extraction kit (Signosis; SK-0001) and mixed with TF Probe mix I and anti-PAK4 antibody (Cell Signaling Technology; 3242). The mixture was analyzed according to the manufacturer's instructions. The activity of each transcription factor was normalized as the fold of GATA's activity.

MEF2 activity assay.

ECs were co-transfected with the pMEF2-fLuc reporter vector (Signosis; LR-2055) and the Renilla-Luc vector using FuGene 6 reagent (Promega; E2693) in serum-free Opti-MEM medium for 6 h, followed by recovery with serum-supplemented medium for 24 h. The activities of firefly and renilla luciferases were detected using a Dual-Luciferase Reporter Assay System (Promega; E1980).

Mouse T cell isolation and transduction.

The rLuc-tdTomato sequence was subcloned into the pMSGV vector (Creative Biolabs). EGFRvIII-specific CAR with 139 scFv was generated with mouse CD8 trans-membrane, CD28, 4-1BB and CD3ζ intracellular regions in an MSGV1 retroviral vector as described previously[35]. Retrovirus was generated by co-transfection of these plasmids or control CAR vector plus pCL-Eco helper plasmid (kindly provided by S. Albelda and M. Leibowitz; University of Pennsylvania) with Phoenix cells using Lipofectamine 2000 Transfection Reagent (Life Technologies; 11668–019).

The retroviral supernatant was collected and filtrated using sterilized filters with 0.45-μm pores, then used to transduce murine T cells. In brief, mouse T cells were isolated from mouse spleens using an EasySep Mouse T Cell Isolation Kit (Stemcell Technologies; 19851). T cells were stimulated with 5 μg ml^{-1} anti-CD3 (1:100; BioLegend; 100302) and anti-CD28 (1:100; BioLegend; 102102) antibodies for 2 d, followed by transduction with the retroviral supernatant in RetroNectin (20 μg ml^{-1}; Takara; T100A)-coated plates. Cells were cultured in RPMI 1640 medium supplemented with 10% FBS, 20 mM HEPES buffer and 50 U ml^{-1} interleukin-2 (Peprotech; 212-12) for 4–7 d.

Detection of CAR expression.

Transduced T cells were stained for surface EGFRvIII CAR expression using goat anti-human F(ab′) 2-biotinylated antibody (Jackson ImmunoResearch; 109-065-006) and streptavidin–Alexa Fluor 647 conjugate (Thermo Fisher Scientific; S32357) as described previously[35]. Untransduced cells from the same donor were stained and used as negative controls. The fluorescence was analyzed using a Canto flow cytometer (BD Biosciences), and the data were analyzed using FlowJo software.

T cell-mediated cytotoxicity assay.

The ability of EGFRvIII-specific CAR-T cells to kill target cells was tested using DELFIA EuTDA Cytotoxicity Reagents (PerkinElmer; AD0116). Briefly, target cells (the mouse glioma cell line GL261 expressing mouse Egfrviii) were labeled with fluorescence-enhancing ligand (BATDA) for 30 min, washed with culture medium and pipetted into a 96-well U-bottom plates at a density of 5×10^3 cells per well. The effector cells (Egfrviii CAR-T cells) were added into each well at different ratios of effector to target cells. The plate was incubated for 2 h in a humidified incubator under a 5% CO_2 atmosphere at 37°C. Plates were centrifuged at 500*g* for 5 min and supernatants were transferred to a 96-well DELFIA plate and combined with europium. The fluorescence was measured in a time-resolved fluorometer. BATDA-labeled target cells alone were cultured in parallel (to assess spontaneous lysis) and in the presence of lysis buffer (to measure maximum lysis). Cytotoxicity for each sample is represented as the percentage of specific release and was calculated using the following formula: percentage of specific release = [(experimental release – spontaneous release)/(maximum release − spontaneous release)] × 100

Statistics and reproducibility.

Unpaired two-tailed Student's *t*-tests (for two groups), analyses of variance (ANOVAs; for more two groups) and Mantel–Cox log-rank tests (for survival analysis) were performed using Prism 8.0 software for statistical analyses between groups, and $P < 0.05$ was considered to represent a statistically significant difference. No statistical method was used to predetermine sample size. No data were excluded from the analyses. The investigators were not blinded to allocation during the experiments and outcome assessment.

Reporting Summary.

Further information on research design is available in the Nature Research Reporting Summary linked to this article.

Extended Data

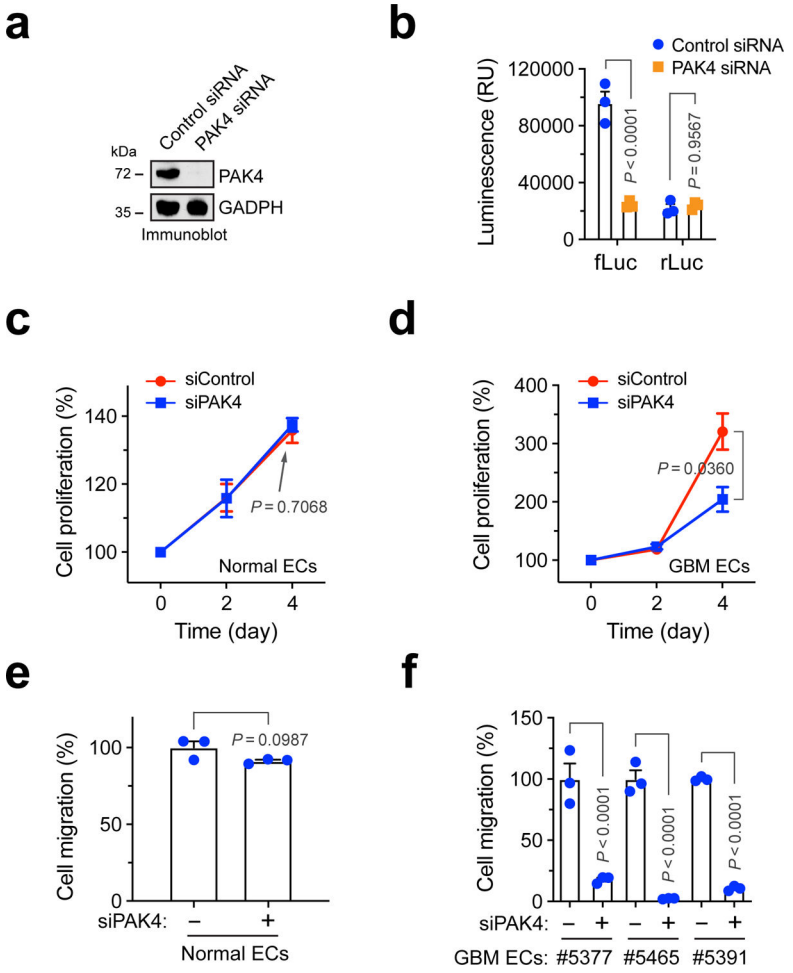

Extended Data Fig. 1 |. Effects of siRNA-mediated PAK4 knockdown on EC functions.
a,**b**, Human GBM-derived ECs from patient #5377 were lentivirally transduced to express SMA-fLuc and CMV-rLuc, followed by transfection with an siRNA targeting PAK4 or a random sequence. **a**, Cell lysates were immunoblotted. This experiment was repeated independently twice with similar results. **b**, Four days after transfection, fLuc and rLuc bioluminescence was analyzed (n = 3 EC samples each derived from a distinct GBM tumor, mean ± SEM). Statistical analysis by two-way ANOVA. **c**-**f**, ECs isolated from human GBM tumors or normal brains were transfection with an siRNA targeting PAK4 or a random sequence. **c**, ECs isolated from normal human brain were subjected to proliferation analysis (n = 3 independent experiments, mean ± SEM). Statistical analysis by two-tailed Student's t test. **d**, GBM ECs isolated from patient #5465 were subjected to proliferation analysis (n = 3 independent experiments, mean ± SEM). Statistical analysis by two-tailed Student's t test. **e**, ECs isolated from normal human brain were subjected to migration analysis (n = 3 EC samples each derived from a distinct GBM tumor, mean ± SEM). Statistical analysis by two-tailed Students' *t*-test. **f**, GBM ECs isolated from three patients were subjected to migration analysis (n = 3 independent assays, mean ± SEM). Statistical analysis by one-way ANOVA.

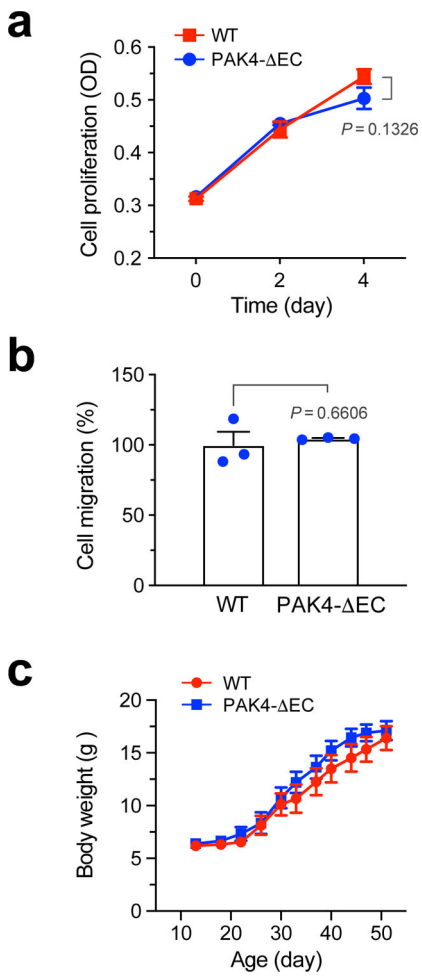

Extended Data Fig. 2 |. Effects of PAK4 knockout on EC proliferation and migration and mouse growth. Ten-day-old *Pak4*$^{fl/fl}$ (WT) and *Cdh5-Cre;Pak4*$^{fl/fl}$ (PAK4-ΔEC) mice were treated with tamoxifen for three days.

a,**b**, Aortic ECs were isolated from 21-day-old mice. **a**, Cell proliferation was determined using a MTT-based assay (n = 5 EC samples each derived from a distinct mouse, mean ± SEM). Statistical analysis by two-tailed Student's t test. **b**, Cell migration in response to FBS was measured using a transwell assay (n = 3 EC samples each derived from a distinct mouse, mean ± SEM). Statistical analysis by two-tailed Students' *t*-tests. **c**, Animal body weight was monitored (mean ± SEM; WT group, n = 4 mice; PAK4-ΔEC group, n = 6 mice).

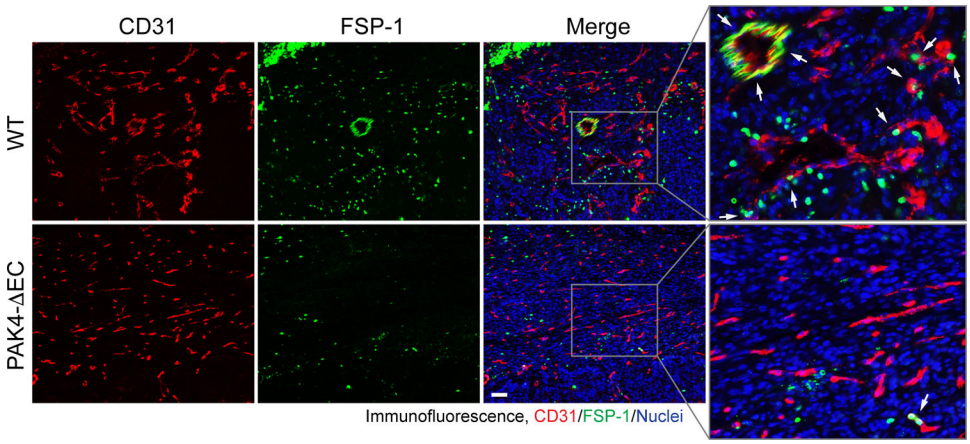

Extended Data Fig. 3 |. PAK knockout in ECs inhibits FSP-1 expression in GBM-associated ECs.
GBM was genetically induced, followed by implantation into WT or PAK4-ΔEC mice. Tumor sections were immunostained using anti-CD31 and anti-FSP-1 antibodies, and subjected to immunofluorescence analysis. Representative images are shown (n = 4 mice). Arrows indicated FSP-1 expression in $CD31^+$ cells. Scale bar: 100 μm.

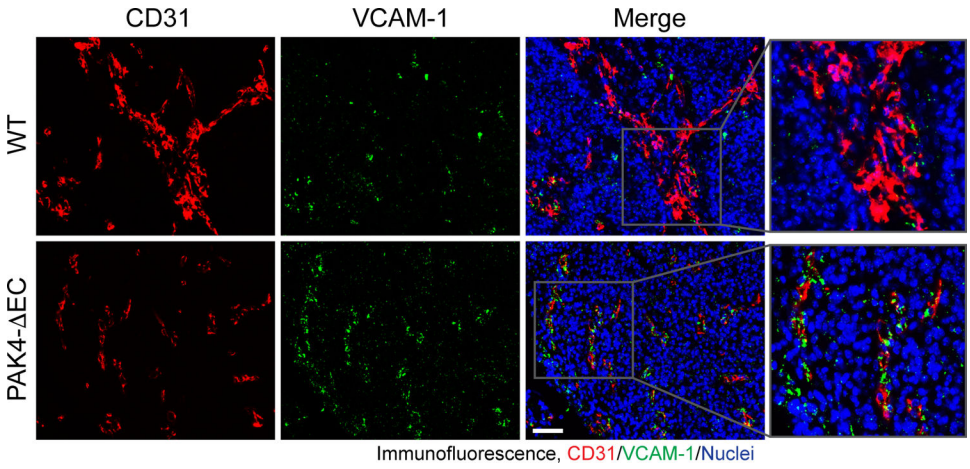

Extended Data Fig. 4 |. PAK4 knockout in eCs restores VCAM-1 expression in GBM-associated eCs.
GBM was genetically induced, followed by transplantation into WT or PAK4-ΔEC mice. Tumor sections were immunostained using anti-CD31 and anti-VCAM-1 antibodies, followed by immunofluorescence analysis. Representative images are shown (n = 4 mice). Scale bar: 100 μm.

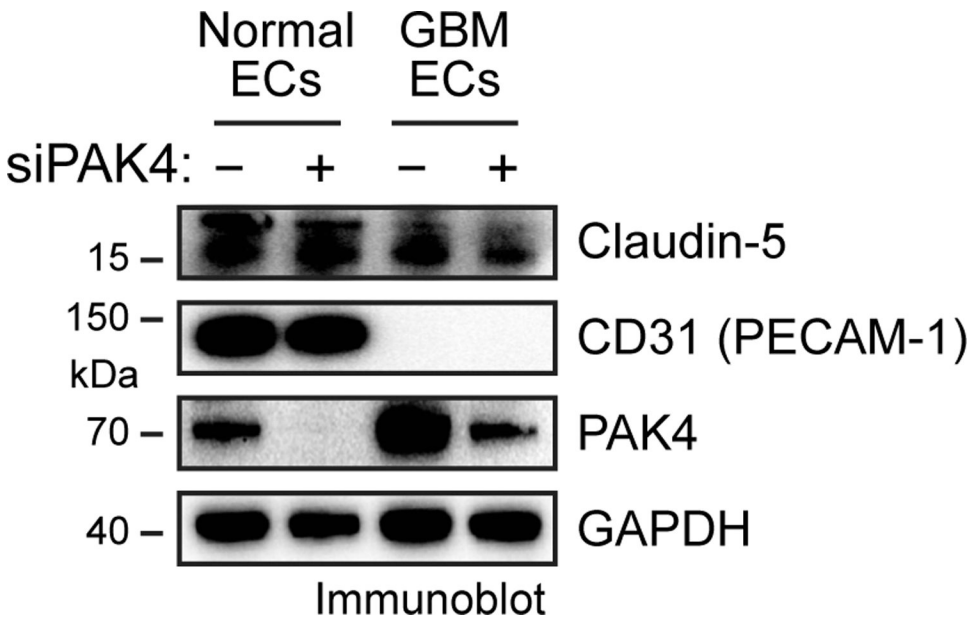

Extended Data Fig. 5 |. PAK4 knockdown did not affect claudin-5 or CD31 expression in GBM ECs and normal ECs.

ECs isolated from human GBM tumor (patient #5377) or normal brain were transfected with siRNA targeting PAK4 or control sequence. Cell lysates were analyzed by immunoblot. This experiment was repeated independently twice with similar results.

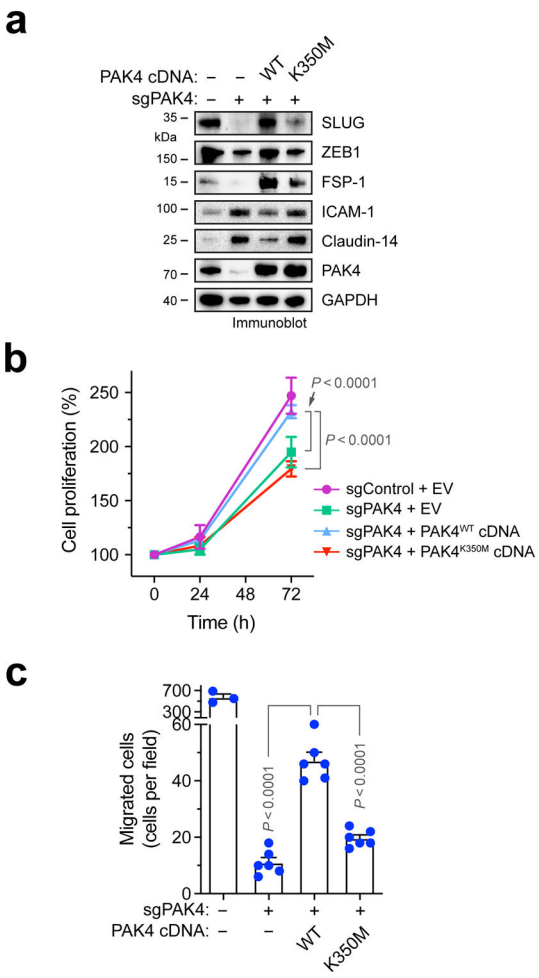

Extended Data Fig. 6 |. PAK4 kinase activity is critical for mesenchymal-like transcriptional reprogramming and cell proliferation and migration in GBM ECs.

ECs isolated from human GBM tumors were transduced to express CRISPR targeting PAK4 or a random sequence, followed by transfection with plasmids expressing WT PAK4 or kinase-dead K350M mutant PAK4 or empty vector (EV). **a**, Cell lysates were analyzed by immunoblot. This experiment was repeated independently twice with similar results. **b**, Cells were subjected to cell proliferation analysis (n = 6 EC samples derived from different tumors, mean ± SD). Statistical analysis by two-way ANOVA. **c**, Cells were subjected to transwell-based cell migration analysis (mean ± SEM, n = 3 EC samples derived from different tumors for control group, and n = 6 EC samples derived from different tumors for other groups). Statistical analysis by one-way ANOVA.

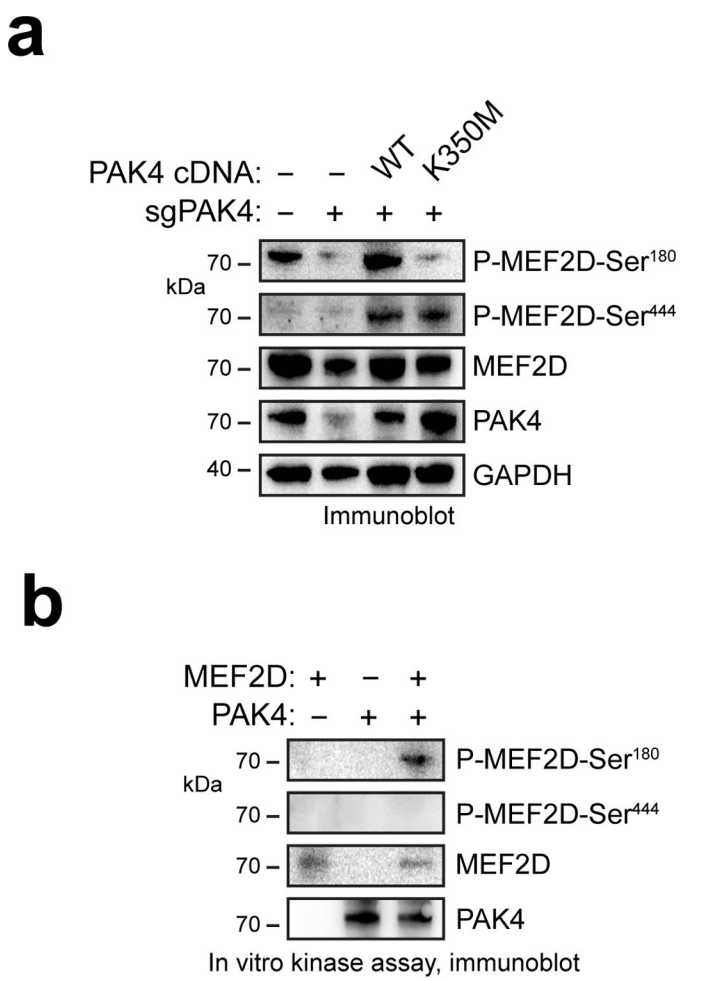

Extended Data Fig. 7 |. PAK4 induces MeF2D phosphorylation at Ser^{180}.
a, ECs isolated from human GBM tumor (patient #5377) were transduced to express CRISPR targeting PAK4 or a random sequence, followed by transfection with plasmids expressing WT PAK4 or kinase-dead K350M mutant PAK4 or empty vector (EV). Cell lysates were analyzed by immunoblot. **b**, Purified MEF2D and PAK4 proteins were incubated in kinase buffer, followed by immunoblot analysis. These experiments were repeated independently twice with similar results.

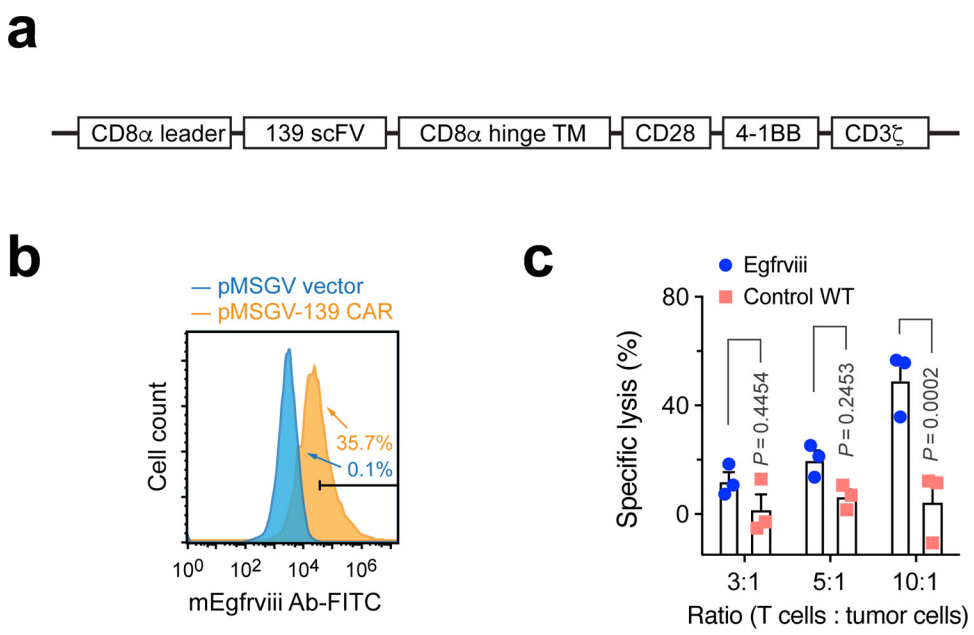

Extended Data Fig. 8 |. A murine Egfrviii CAR T system.

a, Schematic diagram of the mouse Egfrviii CAR T construct. **b**, Mouse spleen-derived T cells were transduced with MSGV retrovirus that encodes Egfrviii 139 CAR or with an empty vector, followed by flow cytometry analysis of 139 CAR expression. Representative cell sortings are shown. **c**, Mouse T cells expressing 139 CAR were incubated with mouse GL261 glioma cells expressing mouse Egfrviii or control WT Egfr. Cell lysis was determined by europium cytotoxicity assay (mean ± SEM, n = 3 T cell samples derived from different mice). Statistical analysis by two-way ANOVA.

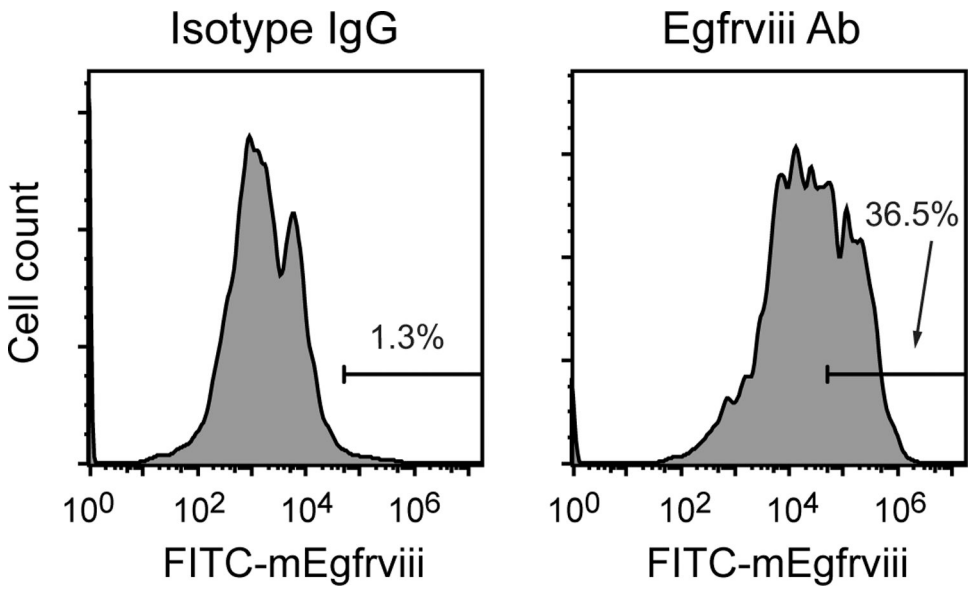

Extended Data Fig. 9 |. Expression of Egfrviii by retroviral transduction in mouse GBM cells.

GBM was genetically engineered induced in mice. Tumor-derived spheres were transduced with retrovirus that expresses mouse Egfrviii, followed by flow cytometry analysis for Egfrviii expression. Representative cell sortings are shown.

Supplementary Material

Refer to Web version on PubMed Central for supplementary material.

Acknowledgements

We are grateful to E. Holland (Fred Hutchinson Cancer Research Center) for providing the RCAS-PDGF GBM model. We thank S. Albelda and M. Leibowitz for help with CAR-T production and G. Linette for helpful discussions. This work was supported in part by the University of Pennsylvania Academic Development Fund (to Y.F.), an Abramson Cancer Center GBM-TCE Award (to Y.F., Z.A.B. and D.M.O.), a RadOnc-TCE Award (to Y.F.), an American Association for Cancer Research Judah Folkman Award (to Y.F.) and National Institutes of Health grants R01NS094533 and R01NS106108 (to Y.F.).

Data availability

RNA-seq data have been deposited in the National Center for Biotechnology Information's Gene Expression Omnibus under accession code GSE154133. The MSigDB database used in the study is available at https://www.gsea-msigdb.org/gsea/msigdb. All of the other data supporting the findings of this study are available from the corresponding authors upon reasonable request. Source data are provided with this paper.

References

1. Carmeliet P & Jain RK Principles and mechanisms of vessel normalization for cancer and other angiogenic diseases. Nat. Rev. Drug Discov 10, 417–427 (2011). [PubMed: 21629292]
2. Weis SM & Cheresh DA Tumor angiogenesis: molecular pathways and therapeutic targets. Nat. Med 17, 1359–1370 (2011). [PubMed: 22064426]
3. Hanahan D & Weinberg RA Hallmarks of cancer: the next generation. Cell 144, 646–674 (2011). [PubMed: 21376230]
4. Lanitis E, Irving M & Coukos G Targeting the tumor vasculature to enhance T cell activity. Curr. Opin. Immunol 33, 55–63 (2015). [PubMed: 25665467]
5. Wang Q et al. Vascular niche IL-6 induces alternative macrophage activation in glioblastoma through HIF-2α. Nat. Commun 9, 559 (2018). [PubMed: 29422647]
6. Huang Y et al. Improving immune–vascular crosstalk for cancer immunotherapy. Nat. Rev. Immunol 18, 195–203 (2018). [PubMed: 29332937]
7. Klein D The tumor vascular endothelium as decision maker in cancer therapy. Front. Oncol 8, 367 (2018). [PubMed: 30250827]
8. Zheng X et al. Increased vessel perfusion predicts the efficacy of immune checkpoint blockade. J. Clin. Invest 128, 2104–2115 (2018). [PubMed: 29664018]
9. Schaaf MB, Garg AD & Agostinis P Defining the role of the tumor vasculature in antitumor immunity and immunotherapy. Cell Death Dis. 9, 115 (2018). [PubMed: 29371595]
10. Batchelor TT et al. AZD2171, a pan-VEGF receptor tyrosine kinase inhibitor, normalizes tumor vasculature and alleviates edema in glioblastoma patients. Cancer Cell 11, 83–95 (2007). [PubMed: 17222792]
11. Jain RK Antiangiogenesis strategies revisited: from starving tumors to alleviating hypoxia. Cancer Cell 26, 605–622 (2014). [PubMed: 25517747]
12. Gilbert MR et al. A randomized trial of bevacizumab for newly diagnosed glioblastoma. N. Engl. J. Med 370, 699–708 (2014). [PubMed: 24552317]

13. Huang M et al. c-Met-mediated endothelial plasticity drives aberrant vascularization and chemoresistance in glioblastoma. J. Clin. Invest 126, 1801–1814 (2016). [PubMed: 27043280]
14. Liu T et al. PDGF-mediated mesenchymal transformation renders endothelial resistance to anti-VEGF treatment in glioblastoma. Nat. Commun 9, 3439 (2018). [PubMed: 30150753]
15. Fan Y Vascular detransformation for cancer therapy. Trends Cancer 5, 460–463 (2019). [PubMed: 31421902]
16. Stupp R et al. Radiotherapy plus concomitant and adjuvant temozolomide for glioblastoma. N. Engl. J. Med 352, 987–996 (2005). [PubMed: 15758009]
17. Huse JT & Holland EC Targeting brain cancer: advances in the molecular pathology of malignant glioma and medulloblastoma. Nat. Rev. Cancer 10, 319–331 (2010). [PubMed: 20414201]
18. Kim KJ et al. Inhibition of vascular endothelial growth factor-induced angiogenesis suppresses tumour growth in vivo. Nature 362, 841–844 (1993). [PubMed: 7683111]
19. Friedman HS et al. Bevacizumab alone and in combination with irinotecan in recurrent glioblastoma. J. Clin. Oncol 27, 4733–4740 (2009). [PubMed: 19720927]
20. Chinot OL et al. Bevacizumab plus radiotherapy–temozolomide for newly diagnosed glioblastoma. N. Engl. J. Med 370, 709–722 (2014). [PubMed: 24552318]
21. Zhao J et al. Immune and genomic correlates of response to anti-PD-1 immunotherapy in glioblastoma. Nat. Med 25, 462–469 (2019). [PubMed: 30742119]
22. O'Rourke DM et al. A single dose of peripherally infused EGFRvIII-directed CAR T cells mediates antigen loss and induces adaptive resistance in patients with recurrent glioblastoma. Sci. Transl. Med 9, eaaa0984 (2017). [PubMed: 28724573]
23. Xie YJ et al. Nanobody-based CAR T cells that target the tumor microenvironment inhibit the growth of solid tumors in immunocompetent mice. Proc. Natl Acad. Sci. USA 116, 7624–7631 (2019). [PubMed: 30936321]
24. Datta M, Coussens LM, Nishikawa H, Hodi FS & Jain RK Reprogramming the tumor microenvironment to improve immunotherapy: emerging strategies and combination therapies. Am. Soc. Clin. Oncol. Educ. Book 39, 165–174 (2019). [PubMed: 31099649]
25. Zeng Q et al. Endothelial cell retraction is induced by PAK2 monophosphorylation of myosin II. J. Cell Sci 113, 471–482 (2000). [PubMed: 10639334]
26. Koh W et al. Formation of endothelial lumens requires a coordinated PKCϵ-, Src-, Pak- and Raf-kinase-dependent signaling cascade downstream of Cdc42 activation. J. Cell Sci 122, 1812–1822 (2009). [PubMed: 19435802]
27. Radu M et al. p21-activated kinase 2 regulates endothelial development and function through the Bmk1/Erk5 pathway. Mol. Cell. Biol 35, 3990–4005 (2015). [PubMed: 26391956]
28. Acloque H, Adams MS, Fishwick K, Bronner-Fraser M & Nieto MA Epithelial–mesenchymal transitions: the importance of changing cell state in development and disease. J. Clin. Invest 119, 1438–1449 (2009). [PubMed: 19487820]
29. Kalluri R & Weinberg RA The basics of epithelial–mesenchymal transition. J. Clin. Invest 119, 1420–1428 (2009). [PubMed: 19487818]
30. Lamouille S, Xu J & Derynck R Molecular mechanisms of epithelial–mesenchymal transition. Nat. Rev. Mol. Cell Biol 15, 178–196 (2014). [PubMed: 24556840]
31. Melder RJ et al. During angiogenesis, vascular endothelial growth factor and basic fibroblast growth factor regulate natural killer cell adhesion to tumor endothelium. Nat. Med 2, 992–997 (1996). [PubMed: 8782456]
32. Griffioen AW, Damen CA, Martinotti S, Blijham GH & Groenewegen G Endothelial intercellular adhesion molecule-1 expression is suppressed in human malignancies: the role of angiogenic factors. Cancer Res. 56, 1111–1117 (1996). [PubMed: 8640769]
33. Hellebrekers DM et al. Epigenetic regulation of tumor endothelial cell anergy: silencing of intercellular adhesion molecule-1 by histone modifications. Cancer Res. 66, 10770–10777 (2006). [PubMed: 17108113]
34. Su L et al. MEF2D transduces microenvironment stimuli to ZEB1 to promote epithelial–mesenchymal transition and metastasis in colorectal cancer. Cancer Res. 76, 5054–5067 (2016). [PubMed: 27364559]

35. Sampson JH et al. EGFRvIII mCAR-modified T-cell therapy cures mice with established intracerebral glioma and generates host immunity against tumor-antigen loss. Clin. Cancer Res 20, 972–984 (2014). [PubMed: 24352643]
36. Sampson JH, Maus MV & June CH Immunotherapy for brain tumors. J. Clin. Oncol 35, 2450–2456 (2017). [PubMed: 28640704]
37. Bovenberg MS, Degeling MH & Tannous BA Cell-based immunotherapy against gliomas: from bench to bedside. Mol. Ther 21, 1297–1305 (2013). [PubMed: 23648695]
38. June CH Principles of adoptive T cell cancer therapy. J. Clin. Invest 117, 1204–1212 (2007). [PubMed: 17476350]
39. Cho JG, Lee A, Chang W, Lee MS & Kim J Endothelial to mesenchymal transition represents a key link in the interaction between inflammation and endothelial dysfunction. Front. Immunol 9, 294 (2018). [PubMed: 29515588]
40. Kovacic JC, Mercader N, Torres M, Boehm M & Fuster V Epithelial-to-mesenchymal and endothelial-to-mesenchymal transition: from cardiovascular development to disease. Circulation 125, 1795–1808 (2012). [PubMed: 22492947]
41. Zeisberg EM et al. Endothelial-to-mesenchymal transition contributes to cardiac fibrosis. Nat. Med 13, 952–961 (2007). [PubMed: 17660828]
42. Li J, Qu X & Bertram JF Endothelial–myofibroblast transition contributes to the early development of diabetic renal interstitial fibrosis in streptozotocin-induced diabetic mice. Am. J. Pathol 175, 1380–1388 (2009). [PubMed: 19729486]
43. Zeisberg EM, Potenta SE, Sugimoto H, Zeisberg M & Kalluri R Fibroblasts in kidney fibrosis emerge via endothelial-to-mesenchymal transition. J. Am. Soc. Nephrol 19, 2282–2287 (2008). [PubMed: 18987304]
44. Chen PY et al. FGF regulates TGF-β signaling and endothelial-to-mesenchymal transition via control of *let-7* miRNA expression. Cell Rep. 2, 1684–1696 (2012). [PubMed: 23200853]
45. Cooley BC et al. TGF-β signaling mediates endothelial-to-mesenchymal transition (EndMT) during vein graft remodeling. Sci. Transl. Med 6, 227ra234 (2014).
46. Maddaluno L et al. EndMT contributes to the onset and progression of cerebral cavernous malformations. Nature 498, 492–496 (2013). [PubMed: 23748444]
47. Eilken HM, Nishikawa S & Schroeder T Continuous single-cell imaging of blood generation from haemogenic endothelium. Nature 457, 896–900 (2009). [PubMed: 19212410]
48. Boisset JC et al. In vivo imaging of haematopoietic cells emerging from the mouse aortic endothelium. Nature 464, 116–120 (2010). [PubMed: 20154729]
49. Kissa K & Herbomel P Blood stem cells emerge from aortic endothelium by a novel type of cell transition. Nature 464, 112–115 (2010). [PubMed: 20154732]
50. Bertrand JY et al. Haematopoietic stem cells derive directly from aortic endothelium during development. Nature 464, 108–111 (2010). [PubMed: 20154733]
51. Lancrin C et al. The haemangioblast generates haematopoietic cells through a haemogenic endothelium stage. Nature 457, 892–895 (2009). [PubMed: 19182774]
52. Krebs AM et al. The EMT-activator Zeb1 is a key factor for cell plasticity and promotes metastasis in pancreatic cancer. Nat. Cell Biol 19, 518–529 (2017). [PubMed: 28414315]
53. Aghdassi A et al. Recruitment of histone deacetylases HDAC1 and HDAC2 by the transcriptional repressor ZEB1 downregulates E-cadherin expression in pancreatic cancer. Gut 61, 439–448 (2012). [PubMed: 22147512]
54. Bolos V et al. The transcription factor Slug represses E-cadherin expression and induces epithelial to mesenchymal transitions: a comparison with Snail and E47 repressors. J. Cell Sci 116, 499–511 (2003). [PubMed: 12508111]
55. Radu M, Semenova G, Kosoff R & Chernoff J PAK signalling during the development and progression of cancer. Nat. Rev. Cancer 14, 13–25 (2014). [PubMed: 24505617]
56. Kesanakurti D et al. A novel interaction of PAK4 with PPARγ to regulate Nox1 and radiation-induced epithelial-to-mesenchymal transition in glioma. Oncogene 36, 5309–5320 (2017). [PubMed: 28534509]

57. Pitts TM et al. Association of the epithelial-to-mesenchymal transition phenotype with responsiveness to the p21-activated kinase inhibitor, PF-3758309, in colon cancer models. Front. Pharmacol 4, 35 (2013). [PubMed: 23543898]
58. Kumar R, Gururaj AE & Barnes CJ p21-activated kinases in cancer. Nat. Rev. Cancer 6, 459–471 (2006). [PubMed: 16723992]
59. Wang K et al. Inhibition of p21 activated kinase enhances tumour immune response and sensitizes pancreatic cancer to gemcitabine. Int. J. Oncol 52, 261–269 (2018). [PubMed: 29115428]
60. Abril-Rodriguez G et al. PAK4 inhibition improves PD-1 blockade immunotherapy. Nat. Cancer 1, 46–58 (2019); erratum 1, 264 (2020). [PubMed: 34368780]
61. Wang Y et al. Ephrin-B2 controls VEGF-induced angiogenesis and lymphangiogenesis. Nature 465, 483–486 (2010). [PubMed: 20445537]
62. Liu Y et al. Somatic cell type specific gene transfer reveals a tumor-promoting function for $p21^{Waf1/Cip1}$. EMBO J. 26, 4683–4693 (2007). [PubMed: 17948060]
63. Ciznadija D, Liu Y, Pyonteck SM, Holland EC & Koff A Cyclin D1 and Cdk4 mediate development of neurologically destructive oligodendroglioma. Cancer Res. 71, 6174–6183 (2011). [PubMed: 21844184]
64. Fan Y et al. Profilin-1 phosphorylation directs angiocrine expression and glioblastoma progression through HIF-1α accumulation. Nat. Cell Biol 16, 445–456 (2014). [PubMed: 24747440]
65. Chung K et al. Structural and molecular interrogation of intact biological systems. Nature 497, 332–337 (2013). [PubMed: 23575631]

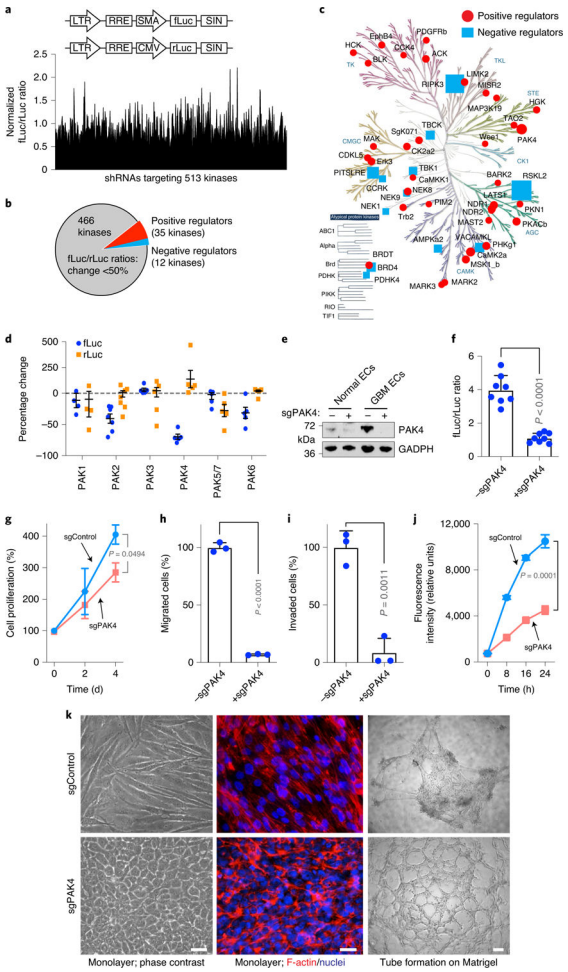

Fig. 1 |. Identification of PAK4 as a critical regulator of mesenchymal-like transcriptional activation and functional abnormalities in GBM ECs.

a–**d**, GBM ECs were lentivirally transduced to express SMA-fLuc and CMV-rLuc, followed by shRNA library-based kinomic screening. fLuc and rLuc bioluminescence was then analyzed. **a**, fLuc/rLuc ratios. LTR, long terminal repeats; RRE, rev response element. **b**, Effects of kinase knockdown on global ratio changes. **c**, Positive and negative regulators denoted in the human kinome. In **b** and **c**, positive regulators indicate ratio decreases of >50% by the kinase knockdown, whereas negative regulators indicate ratio increases of >50% by the kinase knockdown. In **a**–**c**, the values of fLuc/rLuc ratios were averaged. **d**, Effects of PAK family kinase knockdown (means ± s.e.m.; $n = 4$ individual shRNAs for PAK1; $n = 7$ individual shRNAs for PAK2; $n = 5$ individual shRNAs for PAK3, PAK4, PAK5/7 and PAK6). **e**,**f**, ECs isolated from human GBM tumors or from normal brains were lentivirally transduced to express SMA-fLuc, CMV-rLuc and either CRISPR sgRNA targeting PAK4 or a control random sequence. **e**, Cell lysates were immunoblotted. This experiment was repeated independently twice with similar results. **f**, fLuc and rLuc bioluminescence was analyzed in GBM ECs ($n = 8$ independent cell assays; means ± s.e.m.). Statistical significance was determined by two-tailed Student's *t*-test. **g**–**k**, ECs were lentivirally transduced to express CRISPR sgRNA targeting PAK4 or a random sequence. GBM ECs were subjected to proliferation (**g**; means ± s.e.m.), migration (**h**; means ±

s.d.) and invasion analyses (**i**; means ± s.e.m.) (n = 3 EC samples each derived from a distinct human GBM tumor). Statistical significance in **g**–**i** was determined by two-tailed Student's t-test. **j**, GBM ECs were seeded on transwells. FITC-dextran was loaded into the upper chamber and diffused FITC–dextran in the lower chamber was analyzed by fluorospectrometry (n = 3 EC samples, each derived from a distinct human GBM tumor; means ± s.d.). Statistical significance was determined by two-tailed Student's t-test. **k**, GBM ECs were cultured on dishes to form monolayers, then imaged (left) or stained with phalloidin for visualizing F-actin (middle). Right, GBM ECs were seeded on Matrigel for 24 h to form capillary-like tubes. Scale bars, 20 μm. This experiment was repeated independently twice with similar results.

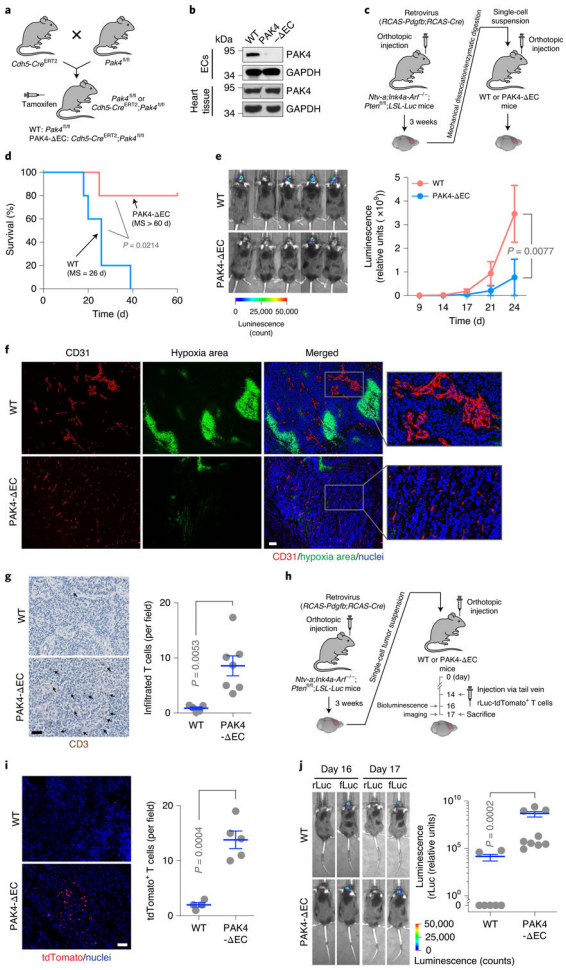

Fig. 2 |. Endothelial-specific deletion of pak4 inhibits vascular abnormalities and enhances t cell infiltration, leading to reduced tumor growth and increased mouse survival.

a,**b**, *Cdh5-Cre*;*Pak4*$^{fl/fl}$ (PAK4-ΔEC) mice were generated by crossing *Cdh5-Cre* mice with *Pak4*$^{fl/fl}$ mice. WT, wild type. **a**, Schematic approach. **b**, ECs were isolated from mouse aortas. Heart tissue and ECs were subjected to immunoblot analysis. This experiment was repeated independently twice with similar results. **c**–**g**, Genetically engineered GBMs were induced, followed by implantation into wild-type or PAK4-ΔEC mice. **c**, Schematic approach. **d**, Animal survival was monitored for 60 d after injection (n = 5 mice). Statistical significance was determined by two-sided log-rank analysis. MS, median survival. **e**, Tumor growth was analyzed by whole-body bioluminescence imaging. Left, representative images at day 17. Right, quantitative analysis of integrated luminescence in tumors (n = 5 mice; means ± s.e.m.). Statistical significance was determined by two-way ANOVA. **f**, Tumor sections were immunostained using anti-CD31 and anti-pimonidazole adduct antibodies. Representative data are shown (n = 4 mice). Scale bar, 100 μm. **g**, Tumor sections were immunostained using an anti-CD3 antibody. Left, representative images. Scale bar, 100 μm. Right, quantitative analysis of CD3$^+$ T cell numbers (means ± s.e.m.; n = 5 mice for the wild-type group; n = 7 mice for the PAK4-ΔEC group). Statistical significance was determined by two-tailed Student's t-test. **h**–**j**, GBM was induced in wild-type or PAK4-ΔEC mice, followed by injection with T cells that were lentivirally transduced to express

rLuc-tdTomato. **h**, Schematic approach. **i**, Tumor sections were immunostained using an anti-tdTomato antibody. Left, representative images are shown. Scale bar, 100 μm. Right, quantified results (means ± s.e.m.; $n = 4$ mice for the wild-type group; $n = 5$ mice for the PAK4-ΔEC group). Statistical significance was determined by two-tailed Student's *t*-test. **j**, Mice were imaged by bioluminescence. Left, representative images. Right, quantitative analysis of integrated rLuc bioluminescence at day 16 (means ± s.e.m.; $n = 7$ mice for the wild-type group; $n = 9$ mice for the PAK4-ΔEC group). Statistical significance was determined by two-tailed Mann–Whitney *U*-test.

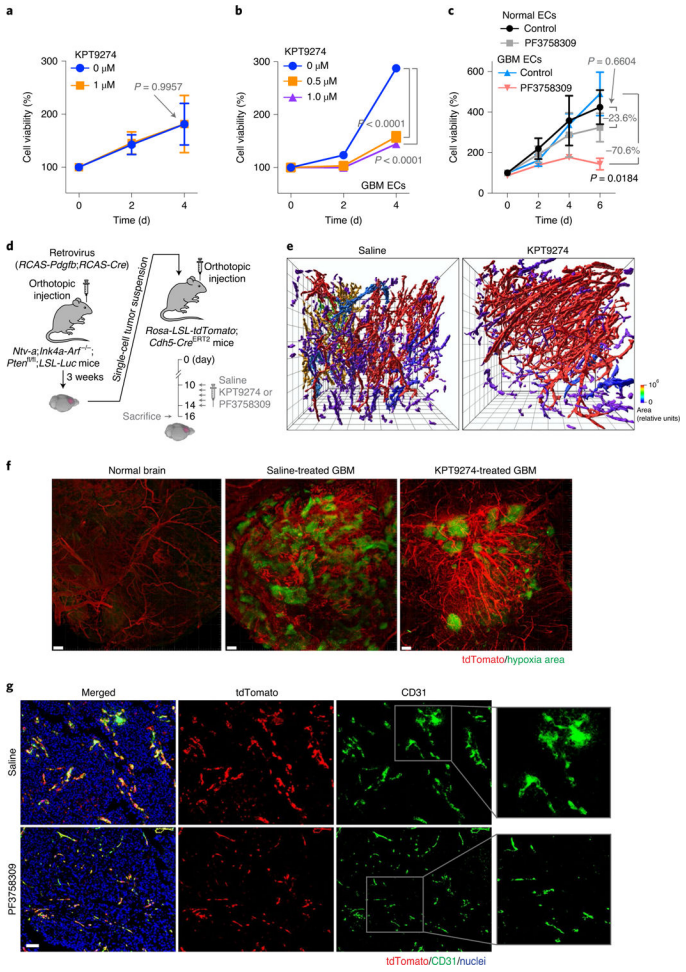

Fig. 3 |. Pharmacological PAK4 inhibition reduces proliferation selectively in GBM ECs and normalizes the tumor vasculature.

a–**c**, ECs isolated from normal human brain or human GBM tumor were treated with the PAK4 inhibitor KPT9274 (0.1–1 μM), the pan-PAK inhibitor PF3758309 (1 μM) or 0.1% dimethyl sulfoxide (control). The cells were then subjected to cell viability analysis. **a**,**b**, Cell viability of normal ECs (**a**) and GBM ECs (**b**) treated with KPT9274 (n = 3 EC samples, each derived from a distinct human GBM tumor; means ± s.e.m.). Statistical significance was determined by two-tailed Student's t-test (**a**) or one-way ANOVA (**b**). **c**, Cell viability of normal and GBM ECs treated with PF3758309 (n = 3 independent experiments; means ± s.e.m.). Statistical significance was determined by two-way ANOVA. **d**–**g**, GBM was induced in *Rosa-LSL-tdTomato*;*Cdh5-Cre*^{ETR2} mice, followed by treatment with saline, KPT9274 (**e** and **f**) or PF3758309 (**g**). **d**, Experimental approach. **e**, Tumors were imaged by light sheet microscopy, followed by three-dimensional reconstruction (n = 3 mice). Each grid, 100 μm. **f**, Whole tumor tissues were stained with an anti-pimonidazole adduct (hypoxia probe) antibody, followed by light sheet fluorescence imaging. Representative images are shown (n = 3 mice). Scale bars, 150 μm. **g**, Tumor sections were stained with anti-tdTomato and anti-CD31 antibodies, followed by immunofluorescence analysis. Representative images are shown (n = 3 mice). Scale bar, 100 μm.

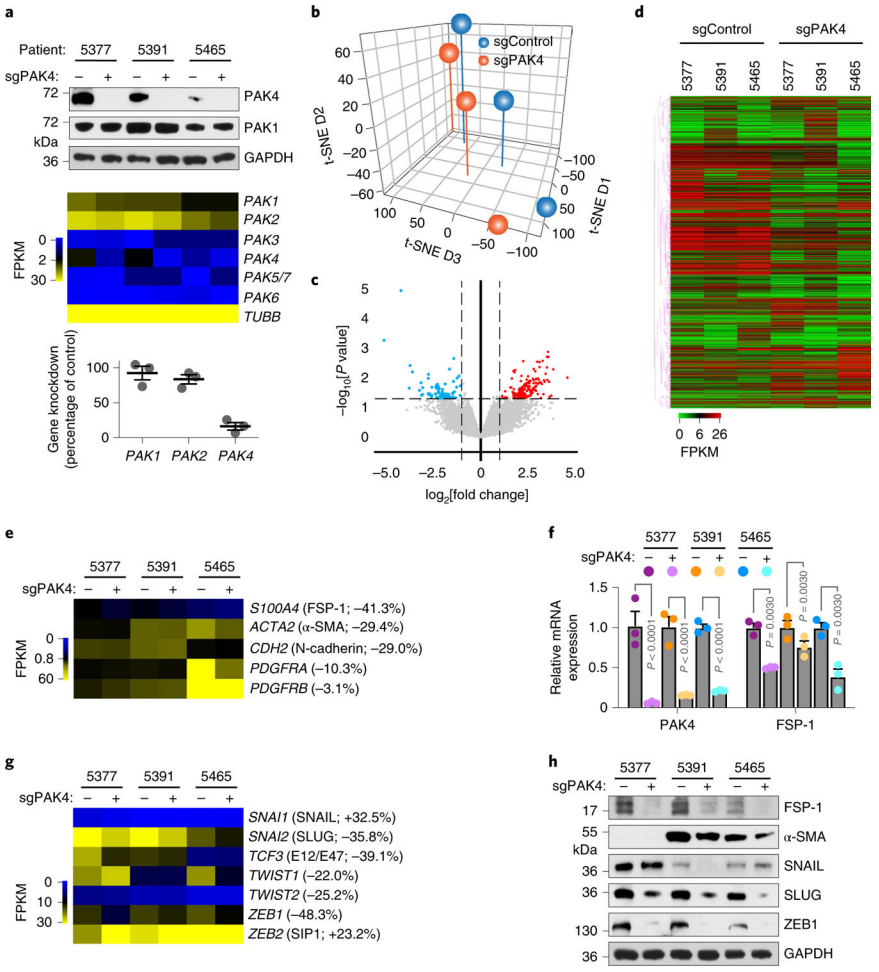

Fig. 4 |. PAK4 is critical for mesenchymal-like transcriptional reprogramming in GBM ECs.

ECs isolated from three human GBM tumors (patients 5377, 5391 and 5465) were transduced to express CRISPR sgRNA targeting PAK4 or a random sequence. Stable sgRNA-expressing ECs were harvested by flow cytometry sorting. **a**–**g**, RNA was extracted and subjected to transcriptome analysis by RNA-seq. **a**, Expression of PAK genes. Top, immunoblot analysis. Bottom, RNA-seq analysis, with quantificaton below (n = 3 EC samples, each derived from a distinct human GBM tumor; means ± s.e.m.). FPKM, fragments per kilobase of transcript per million mapped reads. **b**, t-distributed stochastic neighbor embedding (t-SNE) analysis of all of the mapped genes. **c**, Global change profiles in RNA expression. **d**, Heat map for genes with altered expression (change > 50%), as determined by RNA-seq. **e**, Expression of mesenchymal genes, as determined by RNA-seq. The numbers indicate the average changes in gene expression by PAK4 knockdown. **f**, RNA was isolated and analyzed by quantitative RT-PCR. The results were normalized to GAPDH expression (n = 3 EC samples, each derived from a distinct human GBM tumor; means ± s.e.m.). Statistical significance was determined by two-way ANOVA. mRNA, messenger RNA. **g**, Expression of mesenchymal genes, as determined by RNA-seq. The numbers indicate the average changes in gene expression by PAK4 knockdown. **h**, Cell lysates were immunoblotted. This experiment was repeated independently twice with similar results.

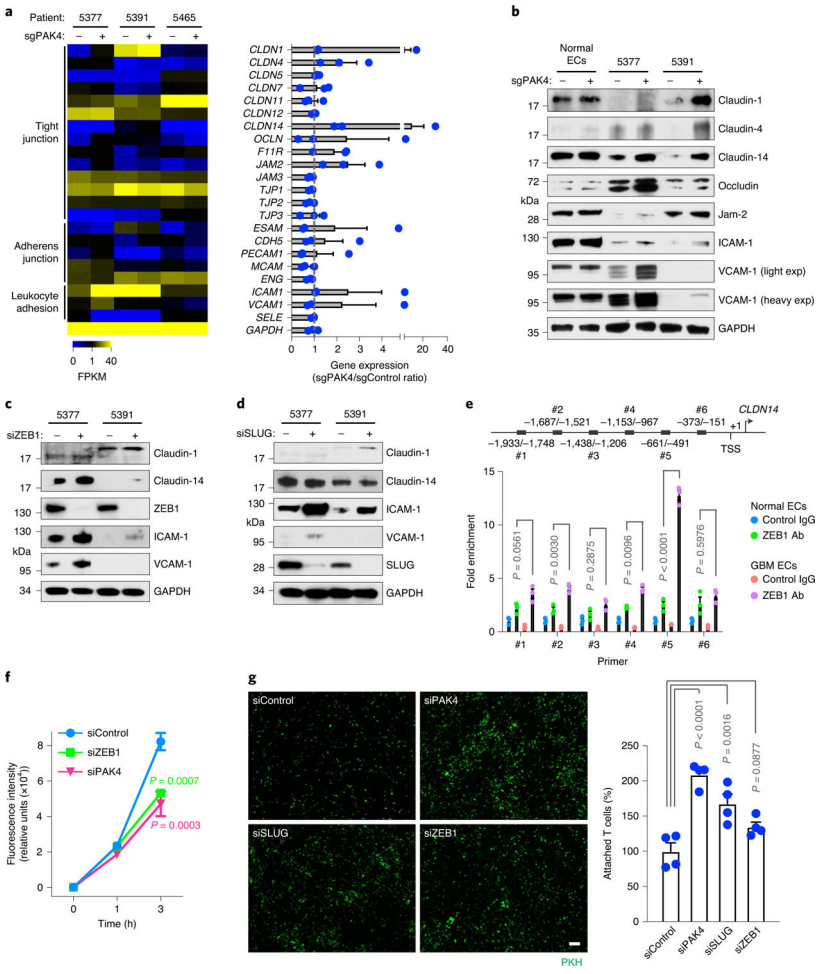

Fig. 5 |. PAK4 suppresses adhesion protein expression via ZEB1 and SLUG, enhancing vessel permeability and reducing T cell adhesion to GBM ECs.

a, ECs were isolated from three human GBM tumors (patients 5377, 5391 and 5465), followed by transduction to express CRISPR sgRNA targeting PAK4 or a random sequence. RNA was extracted and subjected to transcriptome analysis by RNA-seq. Genes associated with tight and adherens junctions were analyzed. Left, heat map. Right, quantitative results (n = 3 EC samples, each derived from a distinct human GBM tumor; means ± s.e.m.). **b**, Human ECs isolated from normal brain or GBM tumors were transduced with lentivirus that expresses CRISPR sgRNA targeting PAK4 or a random sequence. Cell lysates were immunoblotted. **Exp, exposure. c**, Human GBM-derived ECs were transfected with an siRNA targeting ZEB1 or a random sequence, followed by immunoblot analysis. **d**, GBM ECs were transfected with an siRNA targeting SLUG or a random sequence. Cell lysates were immunoblotted. The experiments in **b–d** were repeated independently twice with similar results. **e**, Nuclei extracts from human normal brain ECs or GBM ECs were immunoprecipitated with an anti-ZEB1 antibody or a control antibody, followed by ChIP analysis of ZEB1 binding to the claudin-14 promoter (n = 3 EC samples, each derived from a distinct human GBM tumor; means ± s.e.m.). Statistical significance was determined by two-way ANOVA. Ab, antibody. The numerical values at the top indicate the distance from transcription start site (TSS). **f**, Human GBM-derived ECs were transfected with an

siRNA targeting PAK4, ZEB1 or a random sequence. The cells were seeded on transwells and subjected to monolayer permeability analysis (n = 3 EC samples, each derived from a distinct human GBM tumor; means ± s.e.m.). Statistical significance was determined by one-way ANOVA. **g**, Human GBM-derived ECs were transfected with an siRNA targeting PAK4, SLUG or ZEB1, followed by incubation with PKH-labeled human T cells and imaging. Left, representative images. Scale bar, 50 μm. Right, quantified results (n = 4 T cell samples, each derived from a distinct human donor; means ± s.e.m.). Statistical significance was determined by one-way ANOVA.

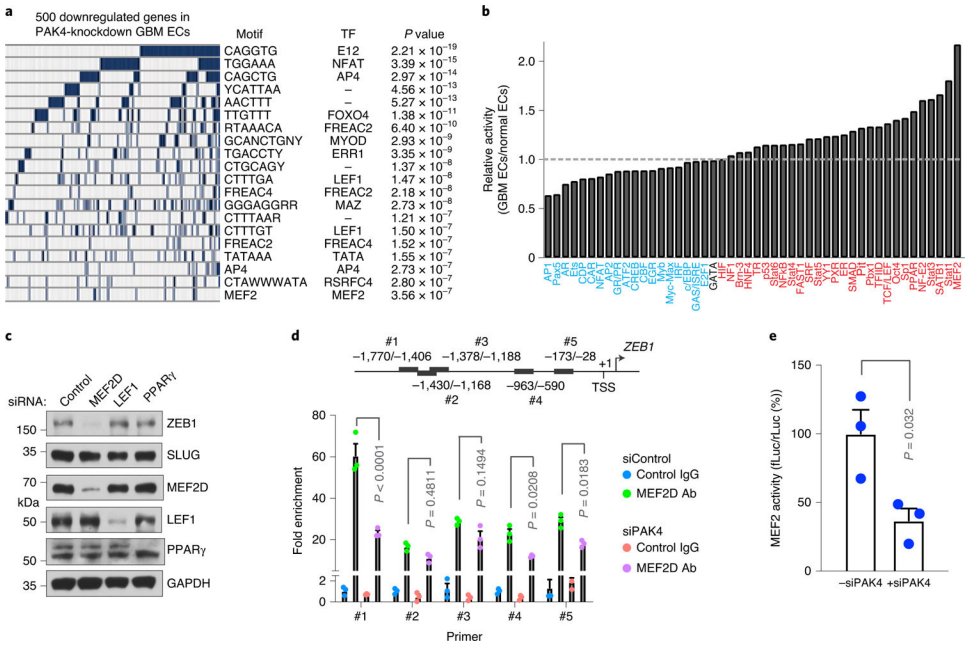

Fig. 6 |. PAK4 induces ZEB1 expression via MEF2D in GBM ECs.

a, Human GBM ECs (n = 3 EC samples, each derived from a distinct human GBM tumor) with or without PAK4 sgRNA treatment were analyzed by RNA-seq. The promoter sequences of downregulated genes were analyzed against the MSigDB database and the most common motifs were identified. The corresponding transcription factors (TFs) are shown. **b**, Nuclei extracts from normal brain ECs or GBM ECs were analyzed using a multiplex transcription factor activity assay. **c**, Human GBM ECs were transfected with an siRNA targeting MEF2, LEF1, PPARγ or a random sequence. Cell lysates were immunoblotted. This experiment was repeated independently twice with similar results. **d**, Human GBM ECs were transfected with siRNA targeting PAK4 or a random sequence. Nuclei extracts were immunoprecipitated using an anti-MEF2 antibody or a control antibody, followed by ChIP analysis of MEF2 binding to the ZEB1 promoter (n = 3 EC samples, each derived from a distinct human GBM tumor; means ± s.e.m.). Statistical significance was determined by two-way ANOVA. **e**, Human GBM-derived ECs were transfected with an siRNA that targets PAK4 or a random sequence. Nuclei extracts were analyzed for MEF2 transcriptional activity (n = 3 EC samples, each derived from a distinct human GBM tumor; means ± s.e.m.). Statistical significance was determined by two-tailed Student's t-test.

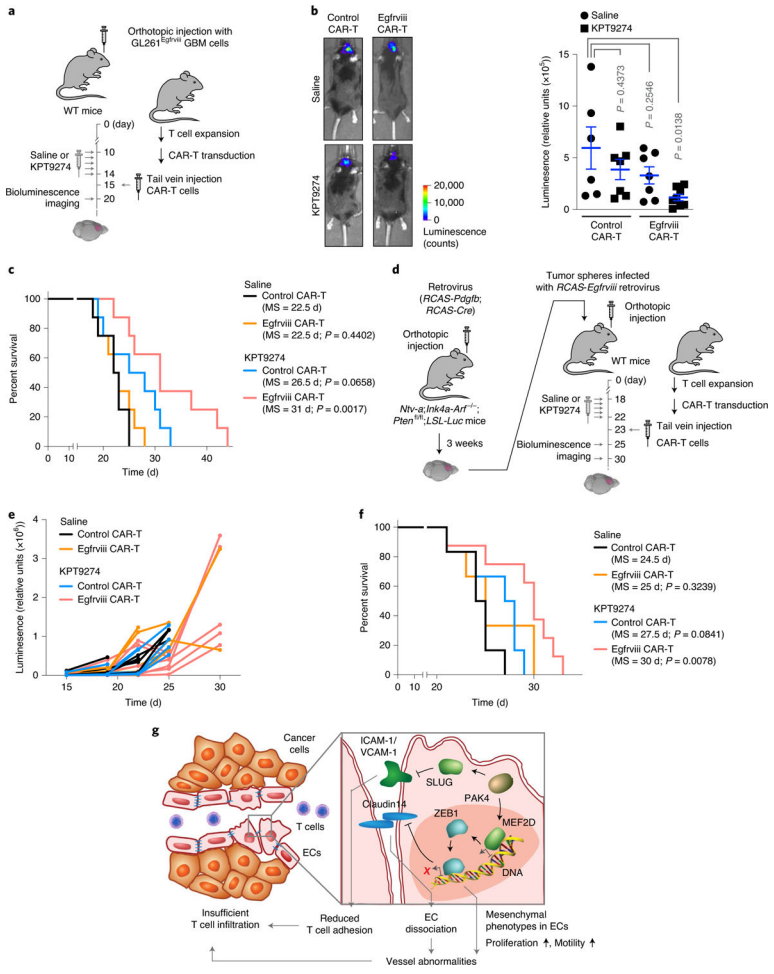

Fig. 7 |. PAK4 inhibition sensitizes GBM to CAR-T immunotherapy.

a–**c**, GL261 GBM was induced in mice, followed by treatment with saline, KPT9274 and/or T cells expressing CAR or a control sequence. **a**, Experimental approach. **b**, At 5 d after injection with CAR-T cells, tumor volumes were analyzed by bioluminescence imaging. Left, representative images. Right, quantitative results (means ± s.e.m.; $n = 6$ mice for the saline + control CAR-T group; $n = 7$ mice for the KPT9274 + control CAR-T group; $n = 7$ mice for the saline + Egfrviii CAR-T group; $n = 8$ mice for the KPT9274 + Egfrviii CAR-T group). Statistical significance was determined by one-way ANOVA. **c**, Animal survival was monitored ($n = 8$ mice). Statistical significance was determined by log-rank analysis. **d**–**f**, GBM was genetically induced in mice. Tumor spheres transduced to express mouse Egfrviii were implanted into mice, followed by treatment with saline, KPT9274 and/or T cells expressing CAR or control sequence. **d**, Experimental approach. **e**, The tumor volume was analyzed by bioluminescence imaging. **f**, Animal survival was monitored. Statistical significance was determined by log-rank analysis ($n = 7$ mice for the KPT9274 + Egfrviii CAR-T group; $n = 5$ mice for the other groups). **g**, Schematic. PAK4 downregulates adhesion protein expression and induces mesenchymal-like transcriptional activation in GBM ECs, driving aberrant vascularization and inhibiting T cell infiltration into tumors.